USGS
science for a changing world

V_{S30} at Three Strong-Motion Recording Stations in Napa and Napa County, California—Main Street in Downtown Napa, Napa Fire Station Number 3, and Kreuzer Lane—Calculations Determined From S-wave Refraction Tomography and Multichannel Analysis of Surface Waves (Rayleigh and Love)

Open-File Report 2018–1161

U.S. Department of the Interior
U.S. Geological Survey

Cover. Photograph showing deployment of refraction cable along Kreuzer Lane in Napa County, California (U.S. Geological Survey photograph by Joanne Chan, 2014).

V_{S30} at Three Strong-Motion Recording Stations in Napa and Napa County, California—Main Street in Downtown Napa, Napa Fire Station Number 3, and Kreuzer Lane—Calculations Determined From S-wave Refraction Tomography and Multichannel Analysis of Surface Waves (Rayleigh and Love)

By Joanne H. Chan, Rufus D. Catchings, Mark R. Goldman, and Coyn J. Criley

Open-File Report 2018–1161

U.S. Department of the Interior
U.S. Geological Survey

U.S. Department of the Interior
RYAN K. ZINKE, Secretary

U.S. Geological Survey
James F. Reilly II, Director

U.S. Geological Survey, Reston, Virginia: 2018

Suggested citation:
Chan, J.H., Catchings, R.D., Goldman, M.R., and Criley, C.J., 2018, V_{S30} at three strong-motion recording stations in Napa and Napa County, California—Main Street in downtown Napa, Napa fire station number 3, and Kreuzer Lane—Calculations determined from s-wave refraction tomography and multichannel analysis of surface waves (Rayleigh and Love): U.S. Geological Survey Open-File Report 2018–1161, 47 p., https://doi.org/10.3133/ofr20181161.

ISSN 2331-1258 (online)

Acknowledgments

We thank the City and County of Napa and Justin Siena High School in Napa, California, for field site access. We thank U.S. Geological Survey (USGS) scientist Joe Svitek and volunteers Coye Slayday-Criley-Brooks, Daniel Brooks, Jeremy Cordova, Rob Huggins, and Adrian McEvilly for assistance in the field. We also thank Jack Boatwright (USGS) and Alan Yong (USGS) for critical reviews.

Contents

Acknowledgments iii
Abstract 1
Introduction 1
Tectonic and Geological Setting 4
August 24, 2014, M_w 6.0 South Napa Earthquake 6
Seismic Survey 7
  Data Acquisition 7
  Profile N15-1—Main Street Downtown Napa (NCSN N016) 7
  Profile N15-2—Napa Fire Station No. 3 (NSMP 1765) 8
  Profile N15-3—Kreuzer Lane (KRE) 10
Seismic-Imaging Methods 10
  Refraction-Tomography Modeling 10
  Multichannel Analysis of Surface Waves (MAS_RW and MAS_LW) 11
V_{S30} Calculations 12
Results 12
  Profile N15-1—Main Street Downtown Napa (NCSN N016) 13
    P-wave Tomography (V_P) Model 13
    S-wave Tomography (V_S) Model 13
    MAS_LW 2D S-wave Velocity Model 14
    MAS_RW 2D S-wave Velocity Model 15
  Profile N15-2—Napa Fire Station Number 3 (NSMP 1765) 16
    P-wave Tomography (V_P) Model 16
    S-wave Tomography (V_S) Model 17
    MAS_LW 2D S-wave Velocity Model 18
    MAS_RW 2D S-wave Velocity Model 19
  Profile N15-3—Kreuzer Lane (KRE) 20
    P-wave Tomography (V_P) Model 20
    S-wave Tomography (V_S) Model 21
    MAS_LW 2D S-wave Velocity Model 22
    MAS_RW 2D S-wave Velocity Model 23
  V_P/V_S Ratios 24
  Poisson's Ratios 25
Summary 25
  V_S Comparison 25
    Profile N15-1—Main Street Downtown Napa (NCSN N016) 25
    Profile N15-2—Napa Fire Station Number 3 (NSMP 1765) 26
    Profile N15-3—Kreuzer Lane (KRE) 26
Conclusion 26
References Cited 27
Appendix 1—Rayleigh and Love Wave Dispersion Curves 32
Appendix 2—Rayleigh and Love Wave Fundamental Mode Dispersion Curve Picks 35
Appendix 3—Rayleigh Wave, Love Wave, and S-Wave Refraction Tomography 1D Velocity-Depth Profiles 38
Appendix 4—V_P/V_S Ratio Determined from P- and S-Wave Refraction Tomography 42
Appendix 5—Poisson's Ratio Determined From P- and S-Wave Refraction Tomography 45

Figures

1. Google Earth satellite image of the San Francisco Bay region, California 3
2. Google Earth image overlain with a geologic map of the Napa Valley, California, study area 5
3. Google Earth satellite image of seismic profile N15-1 on Main Street in downtown Napa, California 8
4. Google Earth satellite image of seismic profile N15-2 at Justin Siena High School in Napa, California 9
5. Google Earth satellite image of seismic profile N15-3 on Kreuzer Lane in Napa, California 10
6. Illustration showing P-wave refraction tomography model for profile N15-1 on Main Street in downtown Napa, California 13
7. Illustration showing S-wave refraction tomography model for profile N15-1 on Main Street in downtown Napa, California 14
8. Illustration showing two-dimensional MAS_LW (multichannel analysis of surface waves for Love waves) shear-wave velocity model for profile N15-1 on Main Street in downtown Napa, California 15
9. Illustration showing two-dimensional MAS_RW (multichannel analysis of surface waves for Rayleigh waves) shear-wave velocity model for profile N15-1 on Main Street in downtown Napa, California 16
10. Illustration showing P-wave refraction tomography model for profile N15-2 at Napa Fire Station Number 3 in Napa, California 17
11. Illustration showing S-wave refraction tomography model for profile N15-2 at Napa Fire Station Number 3 in Napa, California 18
12. Illustration showing two-dimensional MAS_LW (multichannel analysis of surface waves for Love waves) shear-wave-velocity model for profile N15-2 at Napa Fire Station Number 3 in Napa, California 19
13. Illustration showing two-dimensional MAS_RW (multichannel analysis of surface waves for Rayleigh waves) shear-wave velocity model for profile N15-2 at Napa Fire Station Number 3 in Napa, California 20
14. Illustration showing P-wave refraction tomography model for profile N15-3 at Kreuzer Lane (KRE) in Napa County, California 21
15. Illustration showing S-wave refraction tomography model for profile N15-3 at Kreuzer Lane (KRE) in Napa County, California 22
16. Illustration showing two-dimensional MAS_LW (multichannel analysis of surface waves for Love waves) shear-wave velocity model for profile N15-3 at Kreuzer Lane (KRE) in Napa County, California 23
17. Illustration showing two-dimensional MAS_RW (multichannel analysis of surface waves for Rayleigh waves) shear-wave velocity model for profile N15-3 at Kreuzer Lane (KRE) in Napa County, California 24
18. Graphs showing Rayleigh and Love wave dispersion curves representing the point on our seismic profile N15-1: Main Street downtown Napa, California, that is nearest to the strong-motion station 32
19. Graphs showing Rayleigh and Love wave dispersion curves representing the point on our seismic profile N15-2: Napa Fire Station Number 3, Napa County, California, that is nearest to the strong-motion station 33
20. Graphs showing Rayleigh and Love wave dispersion curves representing the point on our seismic profile N15-3: Kreuzer Lane, Napa, California, that is nearest to the strong-motion station 34
21. Graphs showing Rayleigh and Love wave fundamental mode dispersion curve picks across the entire length of the seismic profile N15-1: Main Street downtown Napa, California 35
22. Graphs showing Rayleigh and Love wave fundamental mode dispersion curve picks across the entire length of the seismic profile N15-2: Napa Fire Station Number 3, Napa County, California 36
23. Graphs showing Rayleigh and Love wave fundamental mode dispersion curve picks across the entire length of the seismic profile N15-3: Kreuzer Lane, Napa, California 37

24. Graphs showing Rayleigh wave, Love wave, and S-wave refraction tomography one-dimensional (1D) velocity-depth profiles representing the point on our seismic profile N15-1: Main Street downtown Napa, California, that is nearest to the strong-motion station 38
25. Graphs showing Rayleigh wave, Love wave, and S-wave refraction tomography one-dimensional (1D) velocity-depth profiles representing the point on our seismic profile N15-2: Napa Fire Station Number 3, Napa, California, that is nearest to the strong-motion station....39
26. Graphs showing Rayleigh wave and S-wave refraction tomography one-dimensional (1D) velocity-depth profiles representing the point on our seismic profile N15-3: Kreuzer Lane, Napa County, California, that is nearest to the strong-motion station 40
27. Graphs showing Love wave and S-wave refraction tomography one-dimensional (1D) velocity-depth profiles representing the point on our seismic profile N15-3: Kreuzer Lane that is nearest to the strong-motion station 41
28. Illustration showing the ratio of P-wave velocity to S-wave velocity (V_P/V_S) determined from P- and S-wave refraction tomography along Main Street in downtown Napa, California....42
29. Illustration showing the ratio of P-wave velocity to S-wave velocity (V_P/V_S) determined from P- and S-wave refraction tomography along Napa Fire Station 3, Napa, California....43
30. Illustration showing the ratio of P-wave velocity to S-wave velocity (V_P/V_S) determined from P- and S-wave refraction tomography along Kreuzer Lane (KRE), Napa County, California 44
31. Illustration showing Poisson's ratio determined from P- and S-wave refraction tomography along Main Street in downtown Napa, California....45
32. Illustration showing Poisson's ratio determined from P- and S-wave refraction tomography along Napa Fire Station 3, Napa County, California....46
33. Illustration showing showing Poisson's ratio determined from P- and S-wave refraction tomography along Kreuzer Lane (KRE), Napa, California 47

Tables

1. Peak ground acceleration, peak ground velocity, epicentral distance, and location of three strong-motion stations in Napa County, California, that recorded high PGA values during the 2014 moment-magnitude-6.0 South Napa, California, earthquake 4
2. Parameters for inversion of initial models in multichannel analysis of surface waves for both Rayleigh and Love waves for seismic profiles in Napa County, California....11
3. Time-averaged shear-wave velocity to a depth of 30 meters (V_{S30}) nearest to the strong-motion recording station at each of the three sites in Napa County, California....12

Conversion Factors

International System of Units to U.S. customary units

Multiply	By	To obtain
	Length	
centimeter (cm)	0.3937	inch (in.)
meter (m)	3.281	foot (ft)
kilometer (km)	0.6214	mile (mi)
	Flow rate	
meter per second (m/s)	3.281	foot per second (ft/s)
	Mass	
meter (m)	3.281	foot (ft)
kilogram (kg)	2.205	pound avoirdupois (lb)

Abbreviations

1D	one dimensional
2D	two dimensional
AWD	accelerated weight drop
CMPCC	common mid-point cross-correlation
FZTW	Fault-zone trapped waves
g	acceleration due to gravity at the Earth's surface
Hz	hertz
KRE	Kreuzer Lane
Ma	million years ago or mega-annum
MASW	multichannel analysis of surface waves
MAS_LW	MASW for Love waves
MAS_RW	MASW for Rayleigh waves
M_w	moment magnitude
NCSN	Northern California Seismic Network
NSMP	National Strong Motion Project
PGA	peak ground accelerations
PGV	peak ground velocity
USGS	U.S. Geological Survey
V_P	P-wave or compression-wave velocity
V_S	S-wave or shear-wave velocity
V_{S30}	time-averaged shear-wave velocity in the upper 30 meters of the subsurface
WNFZ	West Napa Fault Zone

V_{S30} at Three Strong-Motion Recording Stations in Napa and Napa County, California—Main Street in Downtown Napa, Napa Fire Station Number 3, and Kreuzer Lane—Calculations Determined From S-wave Refraction Tomography and Multichannel Analysis of Surface Waves (Rayleigh and Love)

By Joanne H. Chan, Rufus D. Catchings, Mark R. Goldman, and Coyn J. Criley

Abstract

The August 24, 2014, moment magnitude (M_w) 6.0 South Napa earthquake caused an estimated $400 million in structural damage to the City of Napa, California. In 2015, we acquired high-resolution P- and S-wave seismic data near three strong-motion recording stations in Napa County where high peak ground accelerations (PGAs) were recorded during the South Napa earthquake. In this report, we present results from three sites—Main Street in Downtown Napa (Northern California Seismic Network station, NCSN N016), Napa Fire Station Number 3 (National Strong Motion Project station, NSMP 1765), and Kreuzer Lane (station KRE, temporary deployment). To characterize the recording sites in terms of shallow-depth shear-wave velocities (V_S), we used both surface waves (Rayleigh and Love) and body waves (S-wave) to evaluate the time-averaged V_S in the upper 30 meters of the subsurface (V_{S30}). We used two-dimensional multichannel analysis of surface waves (MASW) to evaluate V_S from the surface waves, and a refraction tomography inversion algorithm, developed by Hole in 1992, to evaluate V_S from the body waves. As determined by the various methods, we found V_{S30} near the strong-motion recording stations on Main Street in Downtown Napa, Napa Fire Station Number 3, and on Kreuzer Lane to be from 281 meters per second (m/s) to 286 m/s, 297 to 371 m/s, and 885 to 916 m/s, respectively. The V_{S30} calculated from Love waves were slightly lower (10 m/s) than those calculated from Rayleigh waves at the Downtown Napa location and at Napa Fire Station Number 3 (4 m/s); however, V_{S30} calculated from Love waves was higher (190 m/s) than those calculated from Rayleigh waves at Kreuzer Lane. We also found that V_{S30} determined from MASW for both Love and Rayleigh waves varied depending on the number of shots along the profiles, and V_{S30} was not systematic based on the number of shots used in the analysis. Furthermore, V_{S30} calculated from S-wave refraction tomography are closer to those determined from MASW calculated from Love waves than from using Rayleigh waves.

Introduction

In May 2015, we acquired high-resolution seismic profiles near three strong-motion recording stations in the City and County of Napa, California (fig. 1). These three strong-motion stations recorded

horizontal peak ground accelerations (PGAs) ranging from 0.329 *g* (the acceleration due to gravity at the Earth's surface) to 0.611 *g* (table 1), among the highest recorded in the Napa area during the August 24, 2014, moment magnitude (M_w) 6.0 South Napa earthquake. Our goal was to evaluate the seismic velocities of the underlying geologic material at the strong-motion sites using P- and S-wave refraction tomography and analysis of surface waves and to evaluate time-averaged shear-wave velocities (V_S) in the upper 30 meters (m) of the subsurface (V_{S30}) at the sites using methods similar to those used by Catchings and others (2018). In this report, we present results from the three sites—Downtown Napa and Napa Fire Station Number 3, both within the City of Napa, and at the intersection of 4th Avenue and Kreuzer Lane in Napa County.

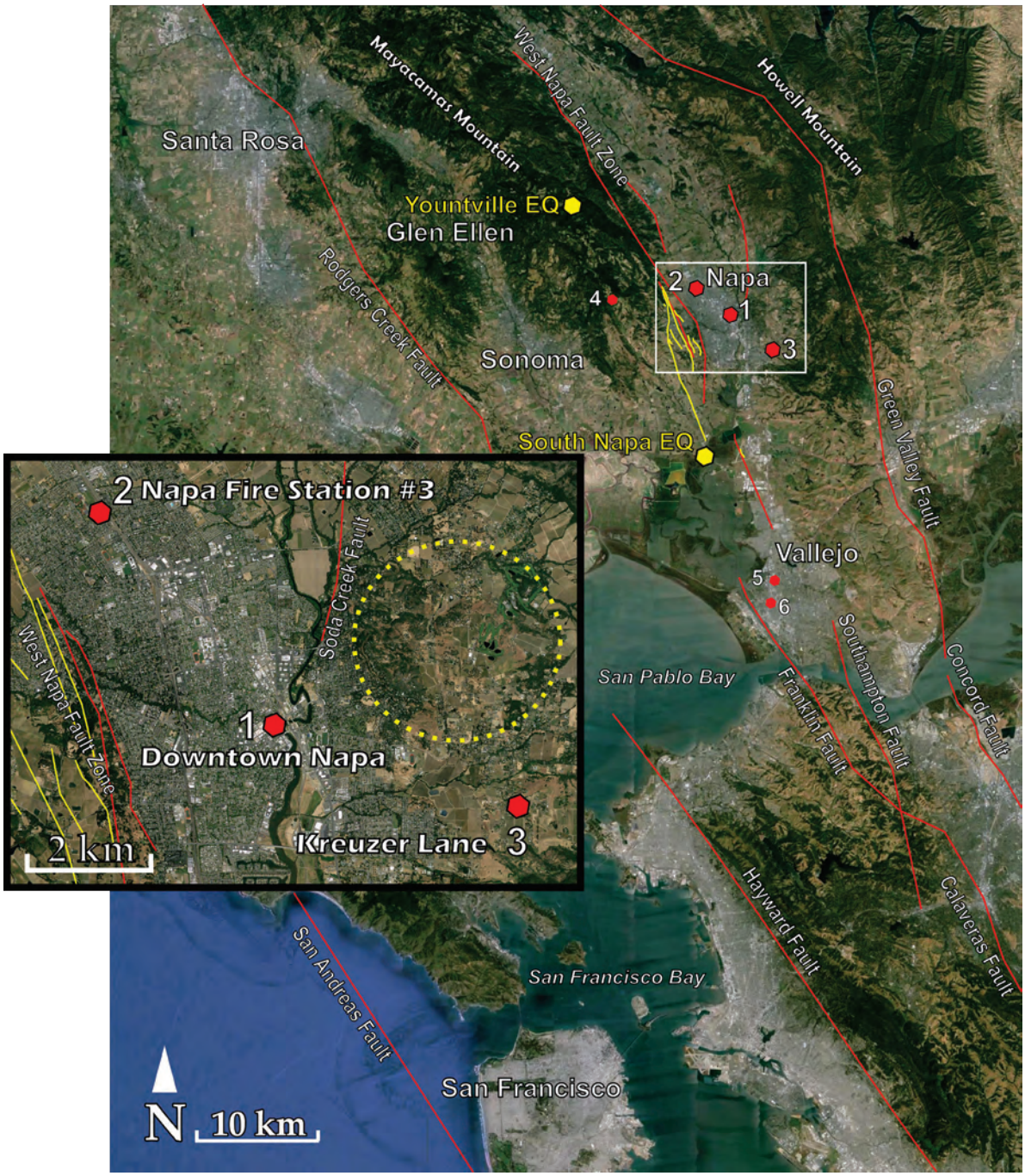

Figure 1. Google Earth satellite image of the San Francisco Bay region, California, showing major faults (red lines), mapped surface ruptures (yellow lines), and the locations (red dots) of our seismic surveys. Yellow dots are the approximate epicenters of the 2000 moment magnitude (M_w) 4.9 Yountville earthquake and the 2014 M_w 6.0 South Napa earthquake. The white box shows the area for the three seismic surveys in Napa County detailed in this report; inset box shows a closer view of this area. Red dot 1 is downtown Napa (seismic profile N15-1), red dot 2 is Napa Fire Station Number 3 (seismic profile N15-2), and red dot 3 is Kreuzer Lane (seismic profile N15-3). Yellow dotted circle is the approximate location of Napa Valley eruptive center (Langenheim and others, 2010). Numbers 4 to 6 are locations of additional seismic surveys described in Chan and others (2018). EQ, earthquake; km, kilometers.

Table 1. Peak ground acceleration (PGA), peak ground velocity (PGV), epicentral distance, and location of three strong-motion stations in Napa County, California, that recorded high PGA values during the 2014 moment-magnitude-6.0 South Napa, California, earthquake (Center for Engineering Strong Motion Center, 2017).
[NCSN, Northern California Seismic Network; NSMP, National strong Motion Project; NA, not applicable]

Station name	Station number	Network	PGA, in centimeters per second	PGV, in centimeters per second	Epicentral distance, in kilometers	Latitude (north)/ longitude (west)
Main Street Napa	N016	NCSN	0.611	47.1	9.1	38.299/122.285
Napa Fire Station Number 3	1765	NSMP	0.427	92.56	12.3	38.330/122.318
Kreuzer Lane (KRE)	NA	NA	0.35	NA	9.5	38.28737/122.242

Napa Valley is located approximately 50 kilometers (km) northeast of San Francisco, California, and is primarily known for its wine industry, which contributes an estimated $13 billion to the local economy and as much as $50 billion to the American economy (Stonebridge Research Group, 2012). Napa County is home to more than 136,000 residents, with more than 76,000 of them living in the City of Napa (U.S. Census, 2010). Geographically, Napa Valley is a structural and topographic depression situated between the Howell Mountains to the east and the Mayacamas Mountains to the west (fig. 1). Within the valley, the surface geology consists dominantly of Quaternary unconsolidated alluvium and is underlain and bordered by late Miocene to Pliocene volcanic rocks and Late Jurassic to Cretaceous Great Valley Sequence, Franciscan Complex rocks, and sediments (Kunkel and Upson, 1960; Howell and Swinchatt, 2000; Wagner and others, 2011). Known faults in the Napa Valley are the West Napa Fault Zone (WNFZ) that trends along the western side of the valley, the Soda Creek Fault, and an unnamed fault to the northeast that trends along the terraces west of and along the foothills of the Howell Mountains (fig. 1). The West Napa Fault is known to be Holocene active (Wagner and others, 2011); it was first mapped by Weaver (1949), and subsequently by others starting in the 1970s (Fox and others, 1973; Helley and Herd, 1977; Graymer and others, 2006). The 2000 M_w 4.9 Yountville earthquake occurred along the WNFZ, and previous studies by Langenheim and others (2006, 2010) suggest the fault has accommodated 5 to 40 km of lateral displacement during the late Neogene and Quaternary. The 2014 South Napa earthquake similarly occurred along the WNFZ, approximately 20 km southeast of the Yountville Earthquake epicenter (fig. 1); both earthquakes caused significant damage in Napa, with more than $400 million in damage to private and commercial properties in 2014. The severity of structural damage caused by the 2014 earthquake resulted from a combination of building age, underlying geology, and basin depth (Boatwright and others, 2015).

Tectonic and Geological Setting

Napa Valley's basin topography began in the late Neogene when the Mendocino triple junction, the northward migration of the transition from subduction to transform motion between the Pacific and North American Plates, passed through the present latitude of Napa. Further basin evolution followed transpressional tectonic forces resulting from three main factors—a vector change in plate motion that began approximately 8 million years ago (mega-annum or Ma) (Atwater and Stock, 2010), Sonoma Volcanic activity between 8 and 2.5 Ma (Wagner and others, 2011), and compressional deformation that extended into the Quaternary (Graymer and others, 2007). Gravity, magnetic, and seismicity studies by Langenheim and others (2010) and Catchings and others (2016) suggest the WNFZ dips steeply to the

southwest and is primarily a right-lateral, strike-slip fault. The westward dip-slip motion along the WNFZ appears to have resulted in the formation of the deepest part of the Napa Valley near downtown Napa (Langenheim and others, 2010; Catchings and others, 2016). The WNFZ may extend northward to the Maacama Fault, and southward, the WNFZ connects to the Franklin Fault, likely extending to the Calaveras Fault; this suggests that the WNFZ and its connecting faults may be approximately 110 km long (Catchings and others, 2016). The Soda Creek Fault is mapped along the southeastern margin of the Napa Valley (fig. 2) and accommodates both horizontal and vertical motion, resulting in more than 200 m of vertical displacement (Weaver, 1949), and it may extend northward to within 2 km of the Maacama Fault near Calistoga, ~40 km northwest of downtown Napa (Langenheim and others, 2010).

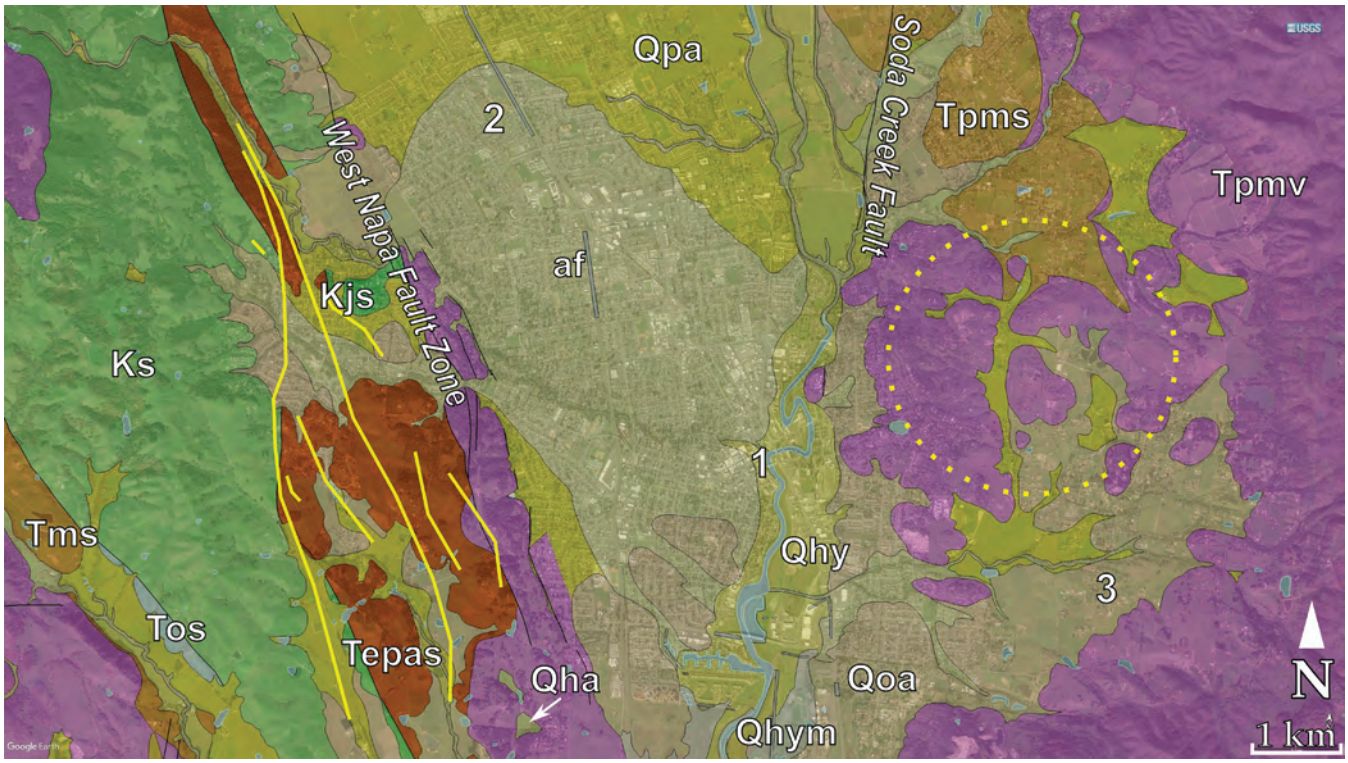

Figure 2. Google Earth image overlain with a geologic map (modified from Graymer and others, 2007) of the Napa Valley, California, study area. Sonoma Volcanics (Tpmv), Neogene sedimentary rocks (Tpms, Tms), Paleogene sedimentary rocks (Tepas), Jurassic to Cretaceous Great Valley sedimentary rocks (KJs, Ks), and Quaternary surficial deposits (Qoa, Qha, Qhy, Qhym, Qpa, af). Gray lines denote Quaternary-active faults, and yellow lines represent surface ruptures mapped after the 2014 moment-magnitude-6.0 South Napa earthquake (Delong and others, 2015). Yellow dotted circle is the approximate location of the Napa Valley eruptive center (Langenheim and others, 2010). See figure 1 for location of map. km, kilometer. 1–3, locations of seismic surveys shown on figure 1.

Late Cenozoic volcanic rocks north of San Pablo Bay are part of a belt of volcanic fields that are younger towards the northwest (Fox and others, 1985a, 1985b). The volcanics are often fault-bounded and displaced dextrally by the fault system on the east side of San Francisco Bay (Graymer and others, 2002). The Sonoma Volcanics include rhyolite, dacite, andesite, basalt, volcanic breccia, glass, and volcanic sand and gravel that were derived from various eruptive sources in the area north of San Francisco Bay (Graymer and others, 2007; Wagner and others, 2011). Pliocene Sonoma Volcanic tuffs are commonly andesitic in composition and are found in the towns of Napa, Sonoma, and Glen Ellen

(Wagner and others, 2011). These tuffs are interpreted as originating from the Napa Valley eruptive center (fig. 1) (Sweetkind and others, 2005). The oldest of the tuffs from the Napa Valley eruptive center is the Pinole Tuff (5.4–5.2 Ma), followed by the tuff of Mark West Springs (5–4.8 Ma), Lawlor Tuff (4.84 Ma), Huichica Tuff (4.71 Ma), and Napa-Healdsburg Tuff (<4.7 Ma) (Wagner and others, 2011).

Mesozoic rocks and sediments of the Franciscan and Great Valley complexes underlie the Sonoma Volcanics in the Napa Valley. The Franciscan Complex originated from Jurassic to Cretaceous oceanic crust and contains graywacke, argillite, basalt, serpentinite, chert, limestone, sandstone, and other high-grade metamorphic rocks (Graymer and others, 2007). The Great Valley Complex consists of Jurassic Coast Range Ophiolite and Jurassic to Cretaceous Great Valley Sequence. The Coast Range Ophiolite outcrops near Lake Berryessa and consists of serpentinite, gabbro, diabase, and basalt, whereas the Great Valley Sequence contains sandstone, shale, and conglomerate (Graymer and others, 2007).

Quaternary surficial deposits cover much of the Napa Valley. These Quaternary deposits are primarily artificial fill, Holocene stream channel deposits, late Pleistocene to Holocene terrace deposits, late Pleistocene to Holocene alluvial fan deposits, early Pleistocene to Holocene alluvium, and bay mud (Knudsen and others, 2000; Graymer and others, 2007). Langenheim and others (2006, 2010) suggest the sedimentary basin beneath the Napa Valley is as deep as 2 km on the basis of gravity data, but recently acquired seismic-refraction data show the basin to be less than 1 km deep (Catchings and others, 2016).

August 24, 2014, M_W 6.0 South Napa Earthquake

The epicenter of the South Napa earthquake was located near American Canyon, approximately 11 km southwest of downtown Napa (fig. 1). The earthquake caused an estimated $400 million in damage to private and commercial properties in the City of Napa (U.S. Geological Survey, 2015). The distribution of red- and yellow-tagged structures in the City of Napa suggests damage highly correlated with buildings that predate 1950; however, damage patterns do not apparently correlate with the underlying geology in Napa (Boatwright and others, 2015). Postearthquake field mapping identified ~12.5 km of surface rupture distributed along subparallel strands of the WNFZ (Brocher and others, 2015; Delong and others, 2015). Overall, more than 30 km of surface deformation was observed from a combination of field observations and geodesy (Delong and others, 2016). Measurements based on alignment arrays and offset features identified up to 50 cm of coseismic slip in the northern section of the rupture and as much as 50 centimeters (cm) of postseismic slip in the southern section approximately one year after the event (Morelan and others, 2015; Lienkaemper and others, 2016). The amount of coseismic and postseismic slip was unusually large for strike-slip earthquakes in California with similar hypocentral depths and magnitudes (Brocher and others, 2015). Earthquake relocation suggests the mainshock and many of the aftershocks occurred near the intersection of two fault planes, one which dips southwest (mainshock) and another northeast (Brocher and others, 2015). Fault-zone trapped waves (FZTWs; also known as guided waves) suggest a low-velocity waveguide along the WNFZ that is at least 400 m in width and 5 to 6 km in depth (Catchings and others, 2016; Li and others, 2016). Furthermore, these studies suggest the greatest reduction in velocity occurs within approximately 200 m of the WNFZ at much shallower depths. The overall length of WNFZ is not well understood; however, postearthquake studies using guided waves (Catchings and others, 2016; Li and others, 2016) and strong-motion data (Baltay and Boatwright, 2015) suggest connectivity between the WNFZ and Franklin Fault, which has been mapped southward to the Calaveras Fault. Furthermore, gravity (Langenheim and others, 2010) and guided-wave (Catchings and others, 2016) studies suggest the

WNFZ may extend northward to the Maacama Fault. Therefore, the combined length of the WNFZ and the Franklin Fault may be nearly 110 km (Catchings and others, 2016).

Seismic Survey

Data Acquisition

In May 2015, we acquired high-resolution P- and S-wave seismic data along linear profiles near strong-motion recording stations in Napa (fig. 1) that recorded high PGAs during the 2014 South Napa Earthquake. As dictated by location and accessibility, we generated P-wave data using one of three active sources—a 226-kilogram (kg) accelerated weight drop (AWD), a 3.5-kg sledgehammer/steel-plate combination, and 400-grain Betsy-Seisgun™ blasts in ~0.4-m-deep boreholes. S-wave sources were generated by horizontally striking an aluminum block with a 3.5-kg sledgehammer. Along each profile, we deployed collocated (1-m offset) P-wave sources and 40-hertz (Hz), vertical-component geophones every 3-m to record P-wave data. We then replaced the vertical-component geophones with 4.5-Hz, horizontal-component geophones and collocated S-wave sources with horizontal-component geophones to record S-wave data. To record the data, we used up to two 60-channel, Geometrics StrataView RX-60™ seismographs that were connected to the geophones via refraction cables (Goldman and others, 2018).

Profile N15-1—Main Street Downtown Napa (NCSN N016)

Profile N15-1 was oriented northwest to southeast on Main Street in downtown Napa between First and Third streets (fig. 3). The strong-motion station (NCSN N016) is housed inside a restaurant on Main Street. To acquire seismic data with minimal cultural noise in the busy downtown corridor, we conducted the survey between 2:00 a.m. and 5:00 a.m. We deployed 48 vertical- and horizontal-component geophones, which were spaced 3-m and coupled to the pavement along profile N15-1. To generate P-waves and S-waves, we used a 226-kg AWD and a 3.5-kg sledgehammer/aluminum-block combination, respectively. The elevation of the geophones along our array varied by approximately 0.5 m over the 141-m length of the seismic profile (Goldman and others, 2018).

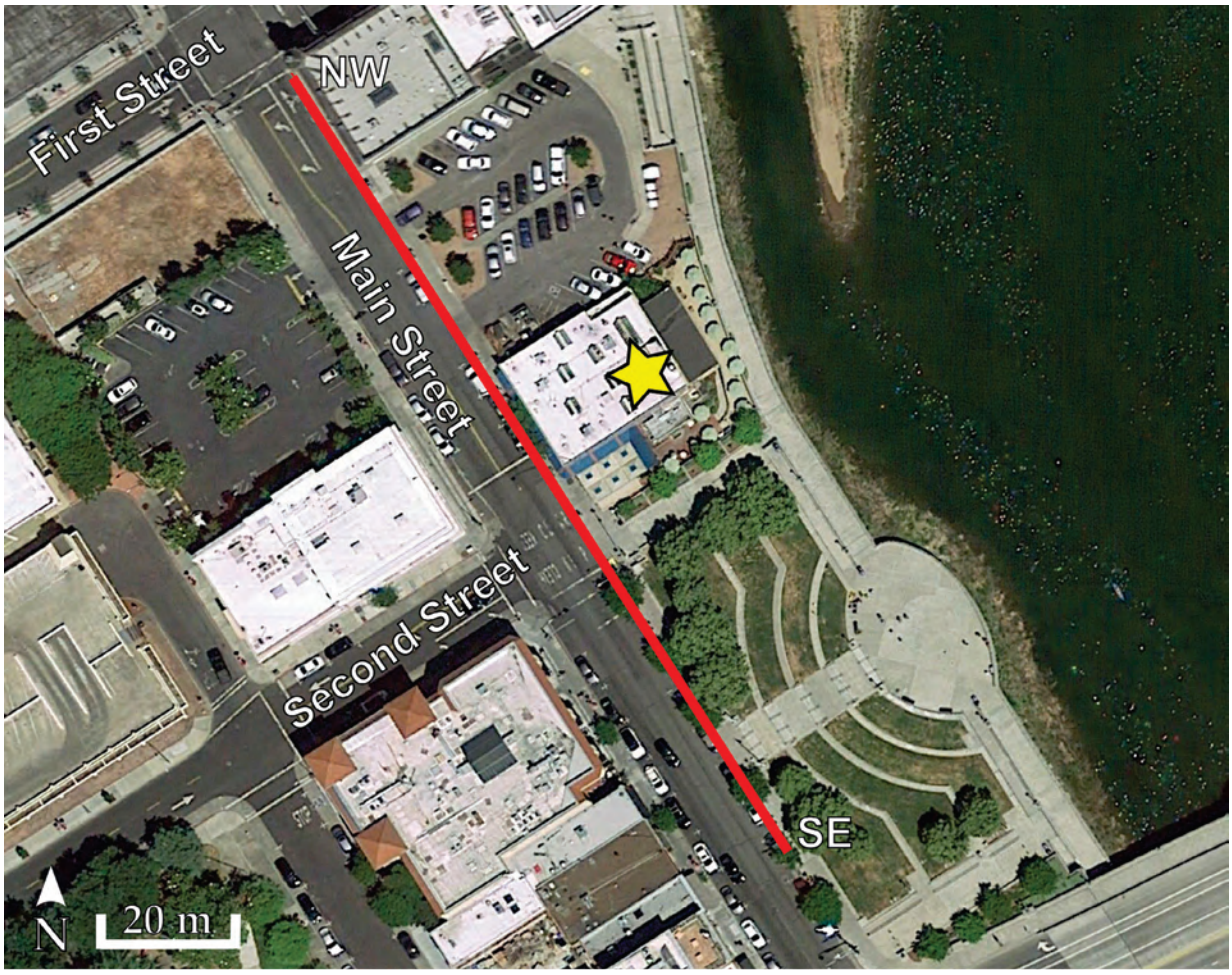

Figure 3. Google Earth satellite image of seismic profile N15-1 on Main Street in downtown Napa, California. Red line represents the seismic profile from northwest to southeast. Yellow star represents the approximate location (meter 60 on seismic profile) of the strong-motion station housed inside Downtown Joe's restaurant on Main Street, Napa. NW, northwest; SE, southeast; m, meters.

Profile N15-2—Napa Fire Station No. 3 (NSMP 1765)

Profile N15-2 was oriented northeast to southwest on the campus of Justin-Siena High School in Napa between the campus track field and Napa Fire Station Number 3 (fig. 4). The strong-motion station (NSMP 1765) was located approximately 20 m east of the seismic profile inside of Napa Fire Station Number 3. We acquired the P- and S-wave data during afternoon hours between about 2:00 p.m. and 7:00 p.m. We deployed 45 vertical- and horizontal-component geophones along profile N15-2, with 3-m spacing between each geophone. To generate P-waves, we used the 226-kg AWD where there was sufficient room to operate the AWD, and we switched to the 3.5-kg sledgehammer/steel-plate combination source where there was not. To generate S-waves, we used the sledgehammer/aluminum-block combination. The geophone elevation varied by approximately 0.9 m over the 132-m length of the seismic profile (Goldman and others, 2018).

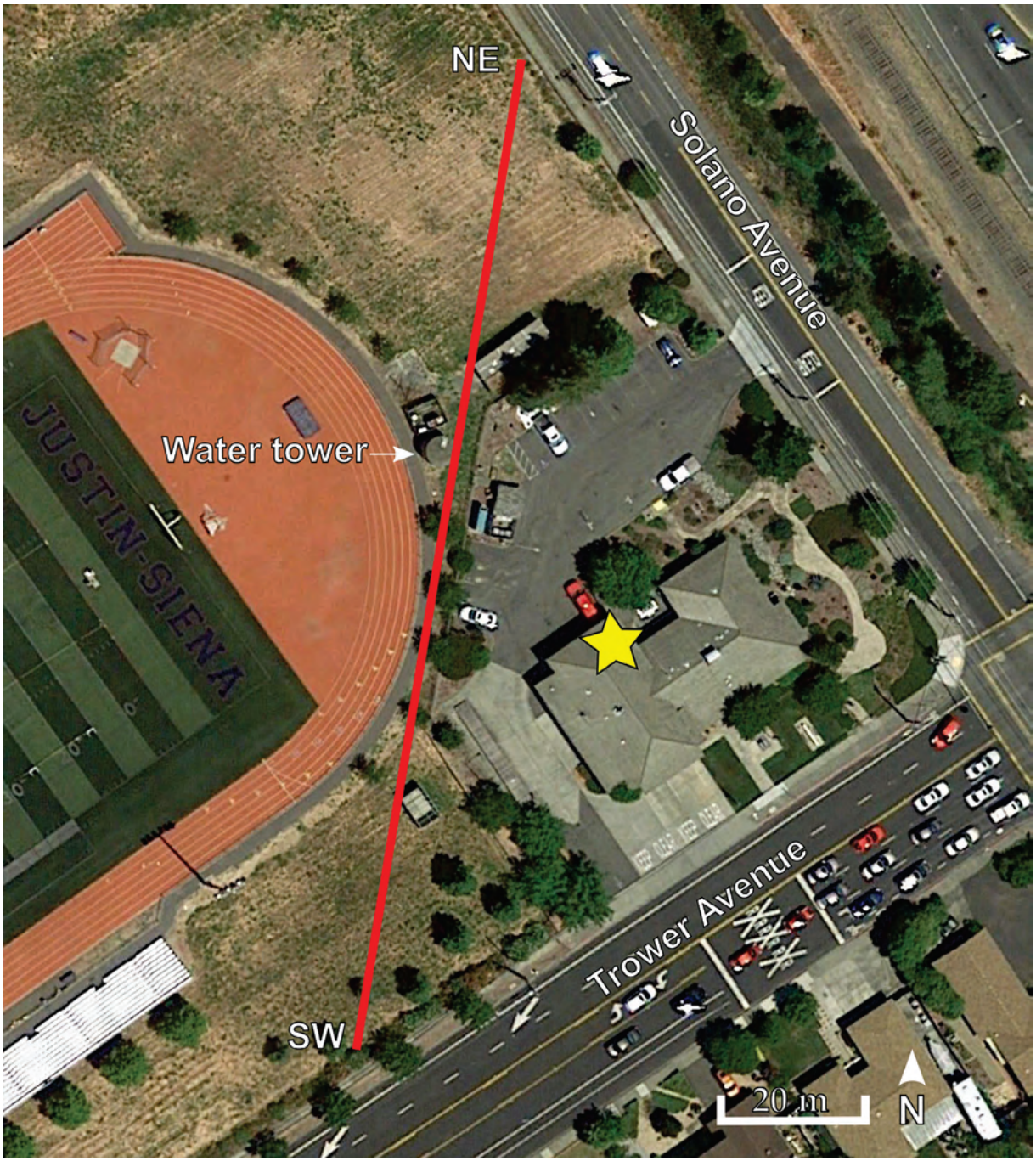

Figure 4. Google Earth satellite image of seismic profile N15-2 at Justin Siena High School in Napa, California. Red line represents the seismic profile from northeast to southwest. Yellow star represents the approximate location (meter 60 on seismic profile) of the strong-motion station housed inside Napa Fire Station Number 3. White arrow points to the leaking water tank adjacent to the seismic line at the time of data acquisition. NE, northeast; SW, southwest; m, meters.

Profile N15-3—Kreuzer Lane (KRE)

Profile N15-3 was oriented west to east on Kreuzer Lane in Napa County, between Curry Lane and Kreuse Canyon Road (fig. 5). The temporary strong-motion station (KRE) was located near the intersection of 4th Avenue and Kreuzer Lane. We deployed 87 vertical- and horizontal-component geophones along profile N15-3, with 3-m spacing between each geophone. As with profile N15-2, we used the 226-kg AWD as our P-wave source, collocated with each geophone. We used the 3.5-kg sledgehammer and aluminum block combination as our S-wave source. The geophone elevation varied by approximately 5 m over the 258-m length of the seismic profile (Goldman and others, 2018).

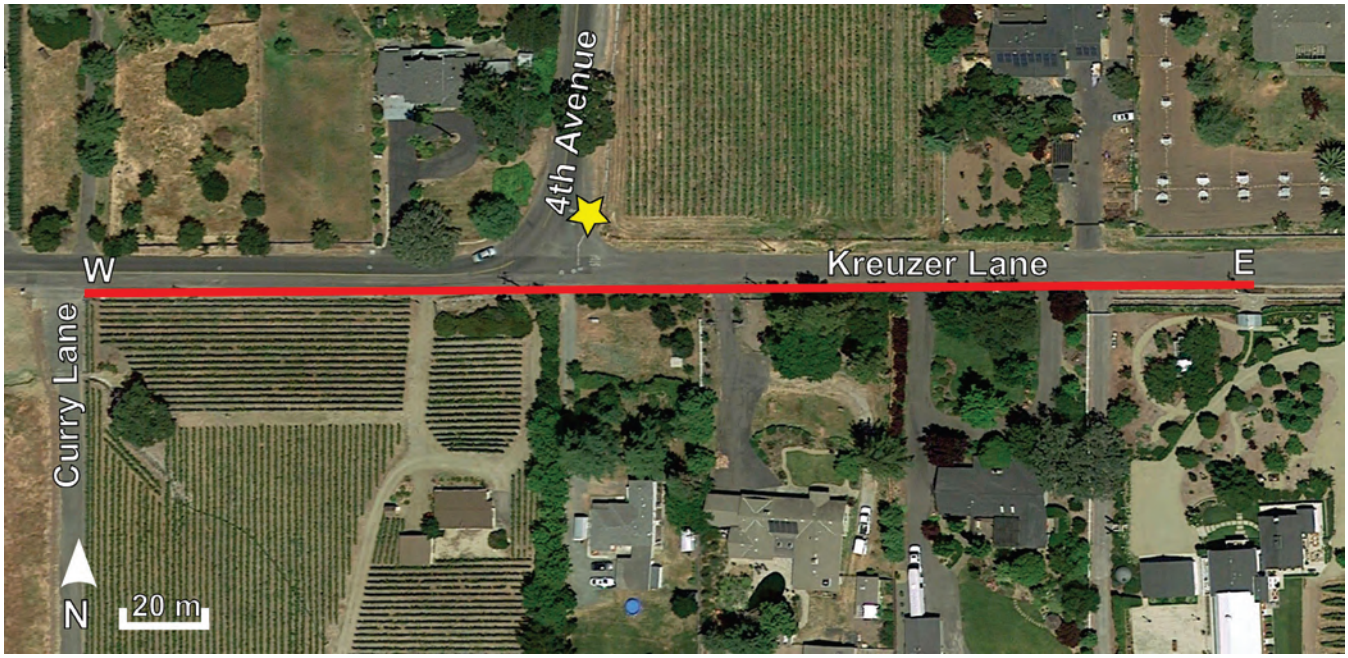

Figure 5. Google Earth satellite image of seismic profile N15-3 on Kreuzer Lane in Napa, California. Red line represents the seismic profile from west to east. Yellow star represents the approximate location (meter 108 on seismic profile) of the strong-motion station near the intersection of Kreuzer Lane and Fourth Avenue. E, east; W, west; m, meters.

Seismic-Imaging Methods

The shoot-through seismic-acquisition method allowed us to develop two-dimensional (2D) P-wave refraction tomography models, S-wave refraction tomography models, and multichannel analysis of surface waves (MASW; Rayleigh-wave, MAS_RW; Love-wave, MAS_LW) models from the recorded data.

Refraction-Tomography Modeling

We used the refraction tomography method to model subsurface P- and S-wave velocities. We first processed the seismic data with ProMax ™, a commercial seismic-processing software (Goldman and others, 2018). First-arrivals from P- and S-wave shot gathers were evaluated and inverted to develop seismic-velocity models using the algorithm of Hole (1992). The algorithm uses finite differences (solving the eikonal equation) to compute first-arrival travel times from the source to the receiver in a starting velocity model. It then uses back-projection of the data misfits to update the model.

This process is repeated in iterative steps until a satisfactory misfit among observed and calculated first-arrivals is obtained. We developed P- and S-wave starting models based on one-dimensional (1D) velocities derived from the shot gathers, and parameterized our initial 2D models into 3-m by 3-m vertical and horizontal grids based on geophone and shot spacing. In modeling, we used 20 to 30 iterations to generate the velocity models. Our P- and S-wave datasets for profiles N15-1 and N15-2 consisted of 2,304 traces (48 shots and 48 geophones) and 2,025 traces (45 shots and 45 geophones), respectively. Profile N15-3 consisted of 6,960 traces (80 shots and 87 geophones) for the P-wave dataset and 7,047 traces (81 shots and 87 geophones) for the S-wave dataset. Generally, the large number of first arrivals used for each profile allows for a well-determined velocity model.

Multichannel Analysis of Surface Waves ($MASW_R$ and $MASW_L$)

Our data acquisition method allows us to use Rayleigh and Love waves to develop 2D S-wave velocity models from P- and S-wave data, respectively, using the MASW method. We used both vertical- and horizontal-component geophones along each profile, which allows for the ability to analyze both Rayleigh and Love waves for V_S. The MASW method takes advantage of the dispersive nature of surface waves to infer shear-wave velocities in the shallow subsurface (Park and others, 1999; Xia and others, 2000). Surface waves are often used in geotechnical site investigations and other shallow subsurface studies (Pujol, 2003; Ivanov and others, 2003, 2013; Miller and others, 1999; Park, 2000, 2013; Odum and others, 2013; Yong and others, 2013). We used the common mid-point cross-correlation (CMPCC) method, developed by Hayashi (2003) and Hayashi and Suzuki (2004), to construct phase velocity (dispersion) curves. We used surface-wave modeling software (SeisImagerSW™, by Geometrics) to iteratively invert the dispersion curves using a non-linear, least-squares approach. Depth is calculated based on one-third of the wavelength, which is determined from dividing the phase velocity by frequency (Hayashi and others, 2016; Geometrics, Inc., 2016). The inversion results of 1D models are combined to construct 2D S-wave velocity models. We varied the number of shots used for the CMPCC method (all shots versus end shots), and we generated additional 2D S-wave velocity models for comparison.

To prepare the data for modeling, P- and S-wave datasets were first converted from SEGY to SEG2 format. We used the SeisImagerSW™ software to construct CMPCC gathers that were then used to calculate phase velocities. To ensure fundamental modes were correctly picked by SeisImagerSW™, we examined and manually adjusted the picks before inversion of the dispersion curves. The starting models (table 2) assume 30-m depth and 10 layers with thickness increasing with depth (Hayashi and others, 2016; Geometrics, Inc., 2016); inverted results may show models at less than or greater than 30-m depth.

Table 2. Parameters for inversion of initial models in multichannel analysis of surface waves for both Rayleigh and Love waves for seismic profiles in Napa County, California.

Seismic profile	Depth, in meters	Number of layers	Layer thickness		Inversion
			Gradient	Bottom layer multiplier	
N15-1	30	10	0.5	3	20
N15-2	30	10	0.5	3	20
N15-3	30	10	0.5	3	20

V_{S30} Calculations

V_{S30} is the time-averaged V_S to a depth of 30 m (International Code Council, Inc., 2009); it is a parameter used to account for site amplification in ground motion models and to characterize site conditions in ground motion prediction equations (GMPEs). V_{S30} is also a parameter used for establishing building codes for seismic safety (Building Seismic Safety Council, 2003). Previous study by Boore and others (2011) shows close correlation between V_{S20} and V_{S30} in California. V_{SZ} given Z is less than 30 m depth is calculated (International Code Council, Inc., 2009) using interpolated shear-wave velocities.

Results

We present velocity results by site to evaluate S-wave velocity structures and V_{S30} from the three methods—S-wave refraction tomography, MAS_LW, and MAS_RW. Appendix 1 shows dispersion curves for Rayleigh (left column) and Love (right column) waves at locations nearest to the strong-motion station at each seismic profile. We varied the number of shots used in the $MAS_{R,L}W$ analysis (CMPCC constructed using all shots in the profile, CMPCC constructed using two end shots, and a single shot gather nearest to the strong-motion station), which affected the distinctness of the fundamental modes from higher modes in the dispersion curves. Appendix 2 shows dispersion curve picks for Rayleigh (red triangles) and Love (blue circles) waves along the entire length of the profiles using various number of shots for $MAS_{R,L}W$ analysis. Dispersion curve picks show variability across the full length of the profiles and differences between Rayleigh and Love waves. Table 3 and figures in appendix 3 show V_{S30} values and 1D velocity-depth profiles nearest to the strong-motion recording stations. Velocities are not well-constrained when few dispersion data are available, and V_{S30} values are determined from interpolated velocities.

Table 3. Time-averaged shear-wave velocity to a depth of 30 meters (V_{S30}) nearest to the strong-motion recording station at each of the three sites in Napa County, California.

[See appendix 3 for one-dimensional velocity-depth profiles that correspond to the V_{S30} shown in this table. *represents time averaged V_{SZ} given Z less than 30 meters depth (International Code Council, Inc., 2009). KRE, Kreuzer Lane; NCSN, Northern California Seismic Network; NSMP, National Strong Motion Project; RMSE, root-mean-square error; 1D, one dimensional; 2D, two dimensional; MAS_LW, multichannel analysis of surface waves for Love waves; MAS_RW, multichannel analysis of surface waves for Rayleigh waves; NA, not applicable; m/s, meters per second]

	N15-1 NCSN N016		N15-2 NSMP 1765		N15-3 KRE	
	V_{S30} (m/s)	RMSE (m/s)	V_{S30} (m/s)	RMSE (m/s)	V_{S30} (m/s)	RMSE (m/s)
S-wave refraction tomography	281	NA	371	NA	916	NA
All shot gathers						
2D MAS_LW	286	3.5	297*	5.8	885*	4.6
2D MAS_RW	296*	14.0	301*	3.7	695*	5.3
End shots						
2D MAS_LW	289	3.4	310*	6.8	914	11.9
2D MAS_RW	314*	3.4	273*	3.4	690*	6.3
Single shot gather						
1D MAS_LW	286*	2.7	311	1.8	787	2.7
1D MAS_RW	278*	2.0	291	1.9	606	2.4

Profile N15-1—Main Street Downtown Napa (NCSN N016)

P-wave Tomography (V_P) Model

Along our Downtown Napa seismic profile (Main Street), P-wave velocities (compressional wave velocity, V_P) range from 600 m/s in the near surface to about 2,400 m/s at 40 m depth (fig. 6). Velocity contours in the upper 8 m show undulations in the southeastern half of the profile, whereas velocity contours between 8 and 25 m depth exhibit a slight concave shape, with the apex located between distance meters 50 and 70 along the profile. The 1,500 m/s contour, which has been shown to coincide with the top of groundwater (yellow contour) in previous refraction tomography studies (Catchings and others, 2001, 2006, 2013, 2014, 2017a, b) is located at approximately 15 m depth.

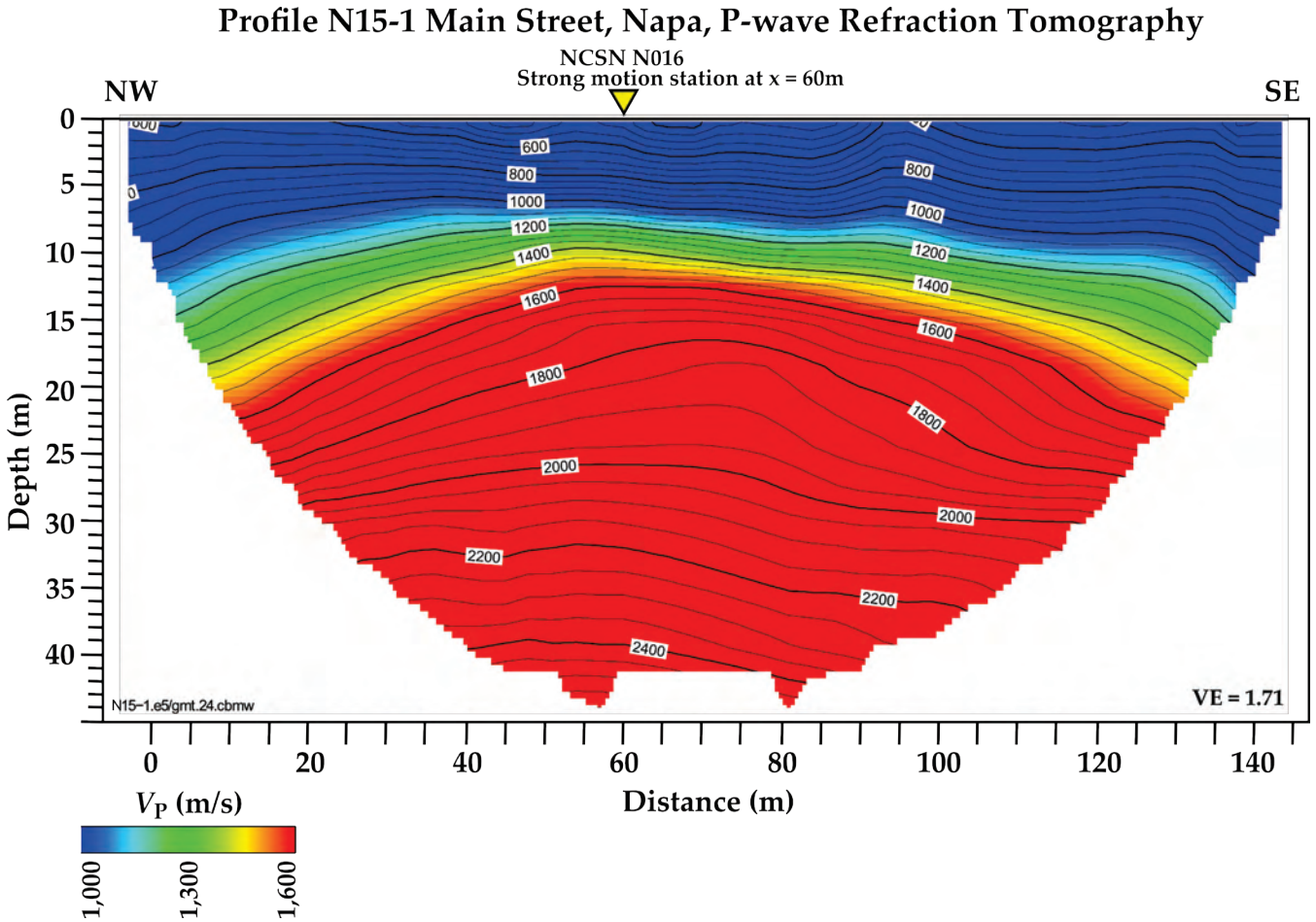

Figure 6. Illustration showing P-wave refraction tomography model for profile N15-1 on Main Street in downtown Napa, California. P-wave velocities range from about 600 meters per second (m/s) in the near surface to 2,400 m/s at 45 meters (m) depth. A concave structure is located near the center of the seismic profile below depths of 5 m. Strong-motion recording station is nearest to distance meter 60 of our seismic profile. NCSN, Northern California Seismic Network; NW, northwest; SE, southeast; VE, vertical exaggeration; V_P, P-wave velocity.

S-wave Tomography (V_S) Model

S-wave velocities (V_S) determined from tomography range from 130 m/s in the near surface to about 400 m/s at 30 m depth (fig. 7). V_S in the upper 15 m of the seismic profile vary only slightly

laterally, and the greater lateral variation in the lower ~10 m when compared to the upper 15 m suggest probable lithological variations. Data coverage reached at least 30 m depth near the center of the tomography model at meter 60, where we calculated V_{S30} to be 281 m/s at the strong-motion station.

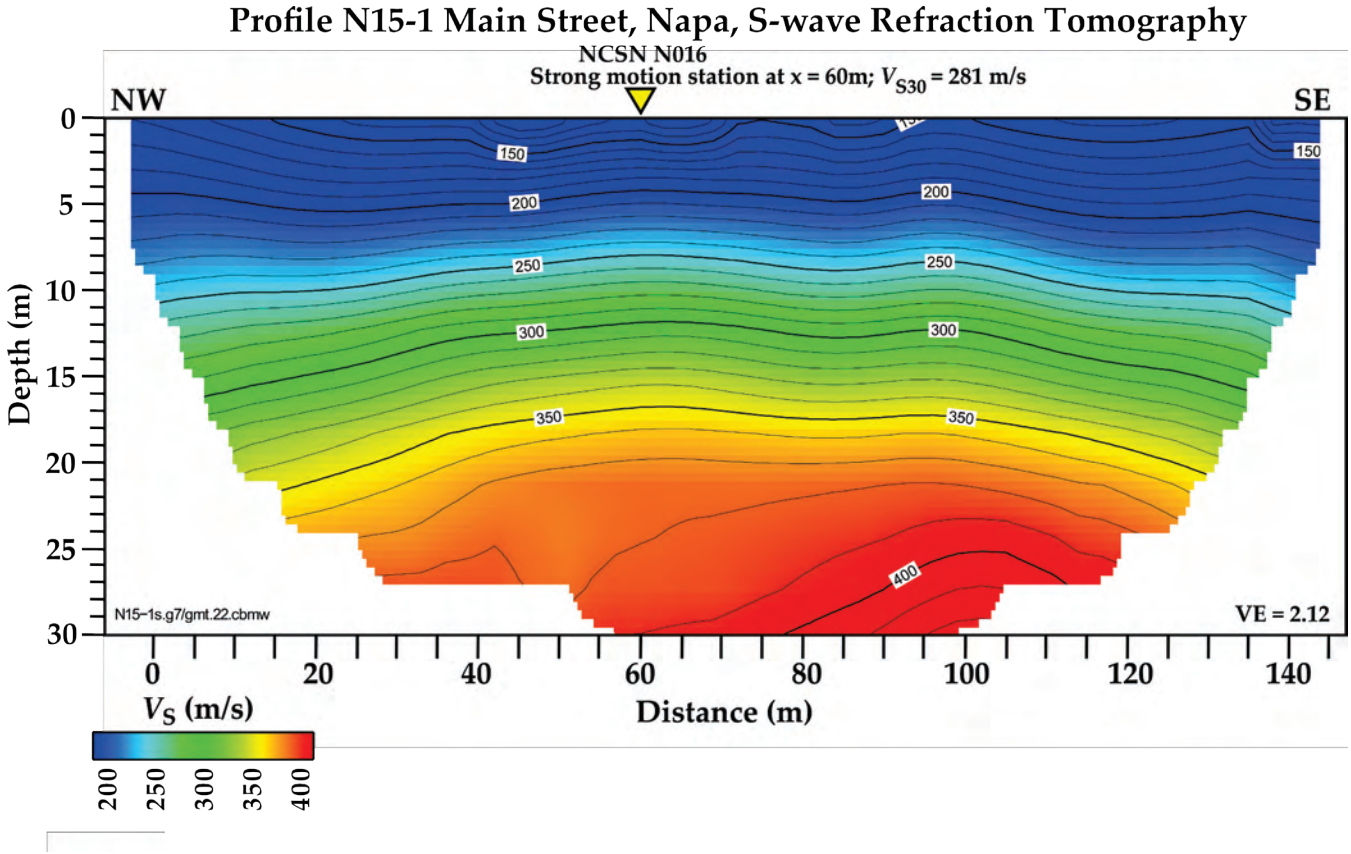

Figure 7. Illustration showing S-wave refraction tomography model for profile N15-1 on Main Street in downtown Napa, California. S-wave velocities range from 150 meters per second (m/s) at the near surface to about 400 m/s at approximately 30 meters (m) depth. Velocity structures are primarily horizontal across the full length of the profile in the upper 20 m but increase in complexity below 20 m. Strong-motion recording station is nearest to distance meter 60 of our seismic profile. NCSN, Northern California Seismic Network; NW, northwest; SE, southeast; VE, vertical exaggeration; V_S, shear-wave velocity; V_{S30}, time-averaged shear-wave velocity in the upper 30 meters of the subsurface.

MASLW 2D S-wave Velocity Model

The Love wave dispersion curves (appendix 1, right column), which represent the location (meter 60) on our seismic profile nearest to the strong-motion recording station, show adjusted picks (red circles) for the fundamental mode at phase velocities between 200 to 400 m/s and at frequencies between 2 to 12 Hz. Love wave dispersion curve picks across the entire length of the profile (appendix 2, blue circles) vary between the number of shots used during CMPCC construction (all shots along the profile versus two end shots) and at each single shot gather along the profile. Table 3 and figures in appendix 3 show V_{S30} and 1D velocity-depth models near the strong-motion station; these results come from using varying MASLW methods—2D MASLW (all shots), 2D MASLW (two end shots), and at a shot gather located at distance meter 60.

Along the Downtown Napa seismic profile, 2D MASLW-determined V_S ranges from 170 m/s in the near surface to about 340 m/s at depth of approximately 25 m (fig. 8). As shown in the P- and S-wave tomography models, there appears to be relatively higher velocities at shallower depths near the center of the profile, forming a broad, concave velocity structure.

We calculated V_{S30} nearest to the strong-motion station at meter 60 along the profile. V_{S30} calculated from 2D MASLW analysis using all shot gathers along the profile is 286 m/s. V_{S30} from 2D MASLW analysis using two end shots is 289 m/s. Finally, V_{S30} at a single shot gather at the strong-motion station is 286 m/s.

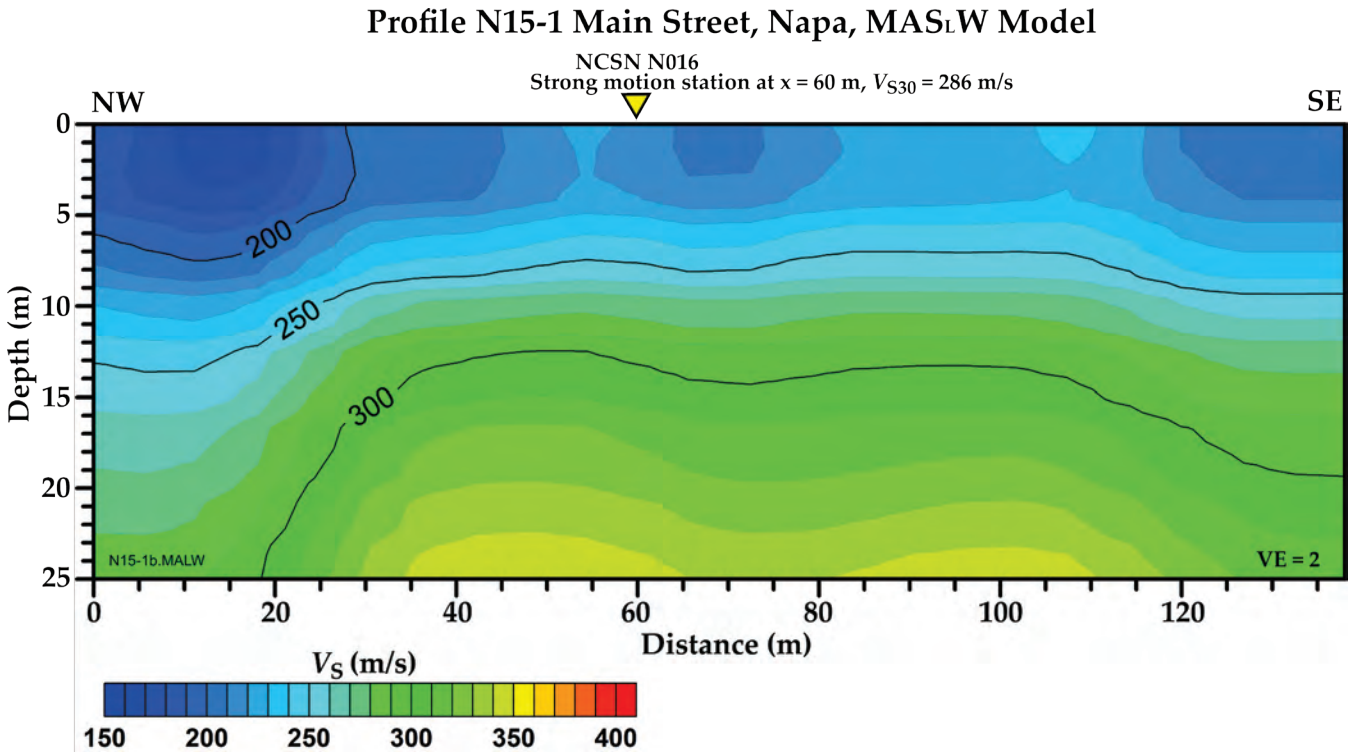

Figure 8. Illustration showing two-dimensional MASLW (multichannel analysis of surface waves for Love waves) shear-wave velocity model for profile N15-1 on Main Street in downtown Napa, California. S-wave velocities range from 170 meters per second (m/s) at the near surface to about 340 m/s at approximately 25 meters (m) depth. Strong-motion recording station is nearest to distance meter 60 of our seismic profile. NCSN, Northern California Seismic Network; NW, northwest; SE, southeast; VE, vertical exaggeration; V_S, shear-wave velocity; V_{S30}, time-averaged shear-wave velocity in the upper 30 meters of the subsurface.

MASRW 2D S-wave Velocity Model

The Rayleigh-wave dispersion curves (appendix 1, left column), which represent the location (meter 60) on our seismic profile nearest to the strong-motion recording station, show adjusted picks (red circles) for the fundamental mode at phase velocities between 200 to 400 m/s and at frequencies between 5 to 15 Hz. The fundamental modes are distinct from higher modes in the dispersion curves. Rayleigh wave dispersion curve picks across the entire length of the profile (appendix 2, red triangles) vary between the number of shots used during CMPCC construction (all shots along the profile versus two end shots) and at each single shot gather along the profile. Table 3 and figures in appendix 3 show V_{S30} and 1D velocity-depth results near the strong-motion station; the results come from using varying

MASRW methods—2D MASRW (all shots), 2D MASRW (two end shots), and at shot gather located at distance meter 60.

Along the Downtown Napa seismic profile, 2D MASRW-determined V_S ranges from 210 m/s in the near surface to about 360 m/s at 25 m depth (fig. 9). The model suggests little horizontal variation in V_S along the seismic profile and only minor variations in the shallow (<5m) subsurface. Generally, the velocities determined from the MASRW technique are slightly higher than those determined from S-wave refraction tomography and from MASLW; however, tomographic velocities are slightly lower in the upper 5 m and slightly higher at about 25 to 30 m depth.

We calculated V_{S30} nearest to the strong-motion station at meter 60 along the profile. V_{S30} calculated from 2D MASRW analysis using all shot gathers along the profile is 296 m/s. V_{S30} from 2D MASRW analysis using two end shots is 314 m/s. Finally, V_{S30} at a single shot gather at the strong-motion station is 278 m/s.

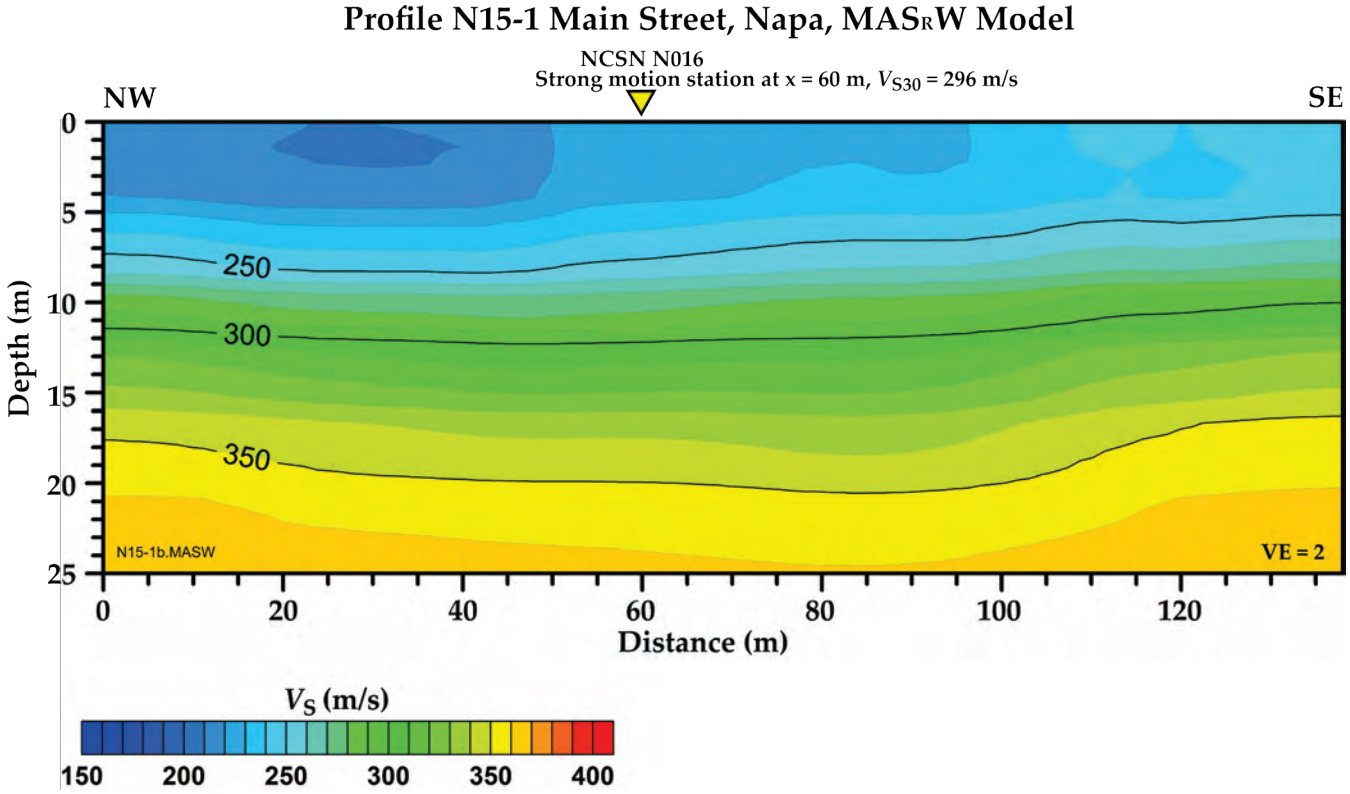

Figure 9. Illustration showing two-dimensional MASRW (multichannel analysis of surface waves for Rayleigh waves) shear-wave velocity model for profile N15-1 on Main Street in downtown Napa, California. S-wave velocities range from 210 meters per second (m/s) at the near surface to about 360 m/s at depth of approximately 25 meters (m). Strong-motion recording station is nearest to distance meter 60 of our seismic profile. NCSN, Northern California Seismic Network; NW, northwest; SE, southeast; VE, vertical exaggeration; V_S, shear-wave velocity; V_{S30}, time-averaged shear-wave velocity in the upper 30 meters of the subsurface.

Profile N15-2—Napa Fire Station Number 3 (NSMP 1765)

P-wave Tomography (V_P) Model

Along our Napa Fire Station Number 3 seismic profile, P-wave velocities range from 600 m/s in the near surface to about 3,000 m/s at depth of approximately 30 m (fig. 10). As seen along profile N15-

1, velocity contours form a pronounced concave shape in the bottom 20 m of the model. The apex is located between distance meters 50 and 100 m of the profile, which coincided with the location of a known leaking water tower (fig. 4) at distance meter 80 at the time of data acquisition. The 1,500 m/s velocity contour (top of groundwater) is located at approximately 8 m depth.

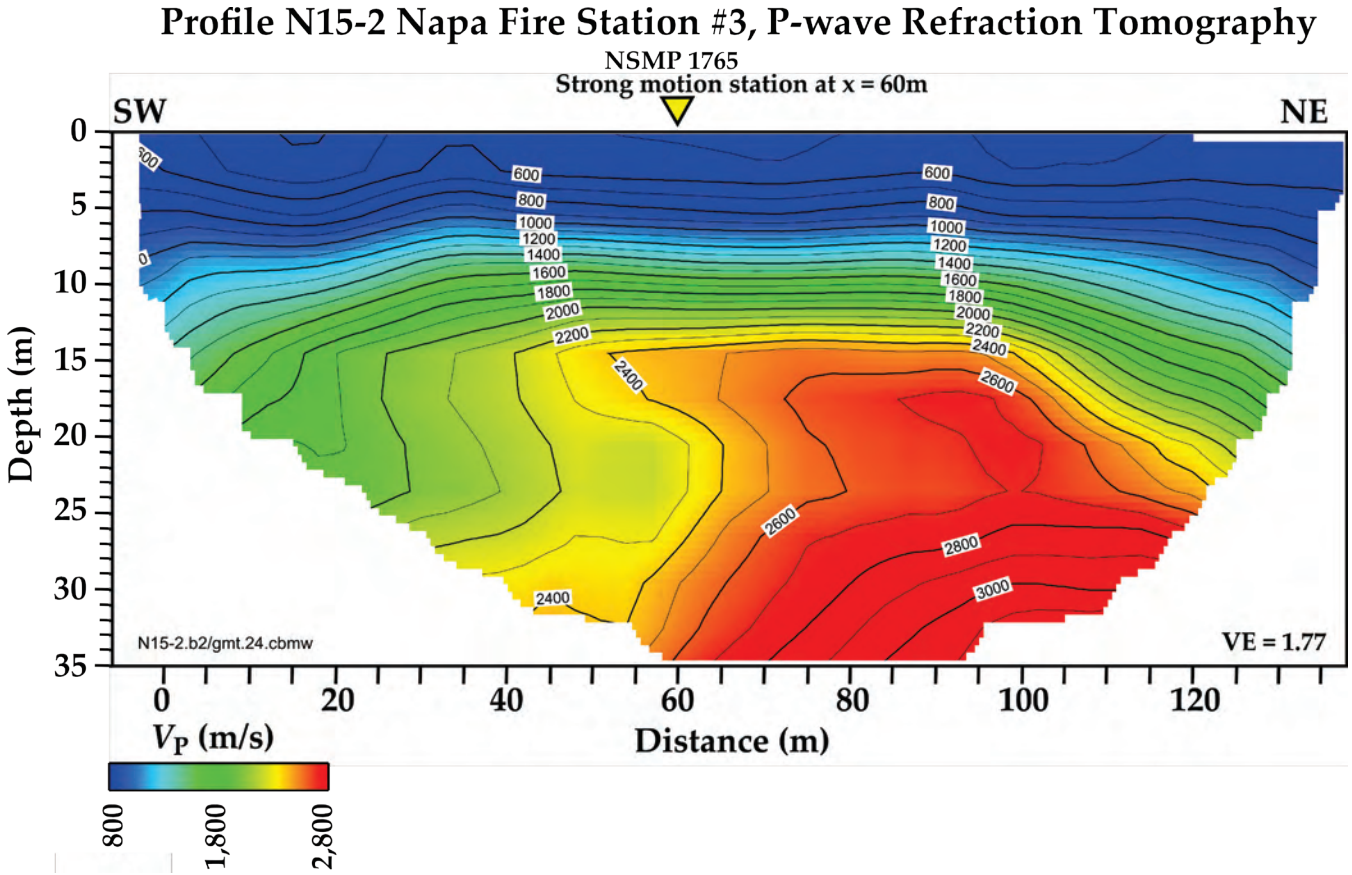

Figure 10. Illustration showing P-wave refraction tomography model for profile N15-2 at Napa Fire Station Number 3 in Napa, California. P-wave velocities range from 600 meters per second (m/s) in the near surface to about 3,000 m/s at 35 meters (m) depth. The location of the leaking water tank (fig. 4) is at distance meter 80. Strong-motion recording station is nearest to distance meter 60 of our seismic profile. NSMP, National Strong Motion Project; NW, northwest; SE, southeast; VE, vertical exaggeration; V_P, P-wave velocity.

S-wave Tomography (V_S) Model

V_S determined from tomography ranges from 220 m/s in the near surface to more than 600 m/s at ~40 m depth (fig. 11). S-wave velocities indicate considerable complexity in structure, lithology, or physical properties of the subsurface along the seismic profile. A slightly southwest-dipping S-wave low-velocity zone is prominent at distance meter 80 of the seismic profile, which coincides with the observed leaking water tank (fig. 4).

Data coverage reached at least 30 m depth between distance meter 30 to meter 117 of the tomography model. Using the tomographic velocity model, we calculated V_{S30} at the strong-motion recording station (meter 60) to be 371 m/s.

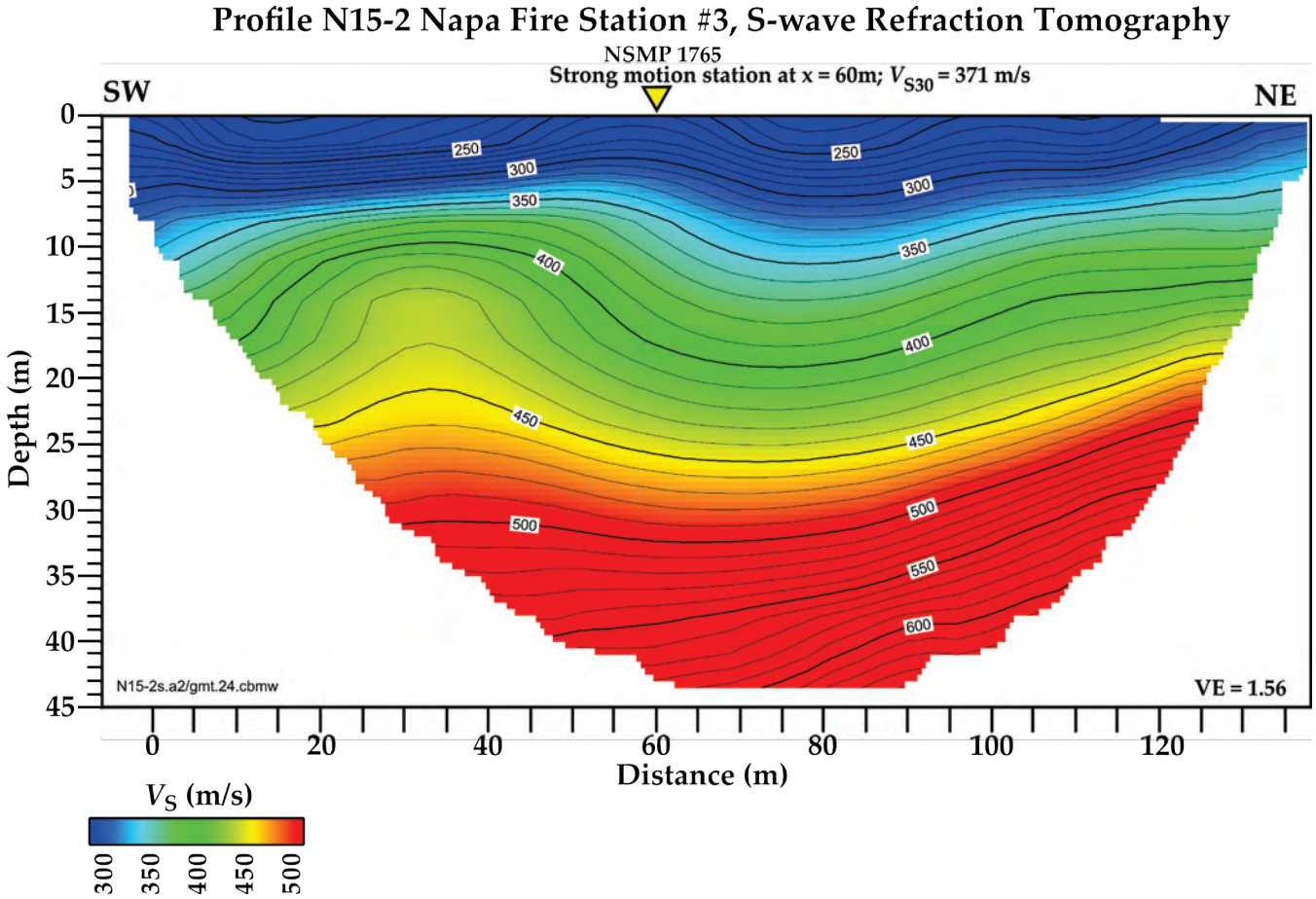

Figure 11. Illustration showing S-wave refraction tomography model for profile N15-2 at Napa Fire Station Number 3 in Napa, California. S-wave velocities range from 250 meters per second (m/s) at the near surface to about 600 m/s at approximately 45 meters (m) depth. The center of the low-velocity zone coincides with the location of the leaking water tank located near distance meter 80 (fig. 4). Strong-motion recording station is nearest to distance meter 60 of our seismic profile. NSMP, National Strong Motion Project; NW, northwest; SE, southeast; VE, vertical exaggeration; V_s, shear-wave velocity; V_{S30}, time-averaged shear-wave velocity in the upper 30 meters of the subsurface.

MAS_LW 2D S-wave Velocity Model

The Love wave dispersion curves (appendix 1, right column), which represent the location (meter 60) on our seismic profile nearest to the strong-motion recording station, show adjusted picks (red circles) for the fundamental mode at phase velocities between 180 to 400 m/s and at frequencies between 3 to 24 Hz. Love wave dispersion curve picks across the entire length of the profile (appendix 2, blue circles) vary between the number of shots used during CMPCC construction (all shots along the profile versus two end shots) and at each single shot gather along the profile. Table 3 and figures in appendix 3 show V_{S30} and 1D velocity-depth results near the strong-motion station; the results come from using varying MAS_LW methods—2D MAS_LW (all shots), 2D MAS_LW (two end shots), and at shot gather located at distance meter 60.

Along the Napa Fire Station Number 3 seismic profile, 2D MAS_LW-determined V_S ranges from 150 m/s in the near surface to about 400 m/s at 20 m depth (fig. 12). The MAS_LW-determined V_S model differs (as much as 100 m/s lower) from that determined from S-wave refraction tomography.

We calculated V_{S30} nearest to the strong-motion station at meter 60 along the profile. V_{S30} calculated from 2D MASLW analysis using all shot gathers along the profile is 297 m/s. V_{S30} from 2D MASLW analysis using two end shots is 310 m/s. Finally, V_{S30} at a single shot gather at the strong-motion station is 311 m/s.

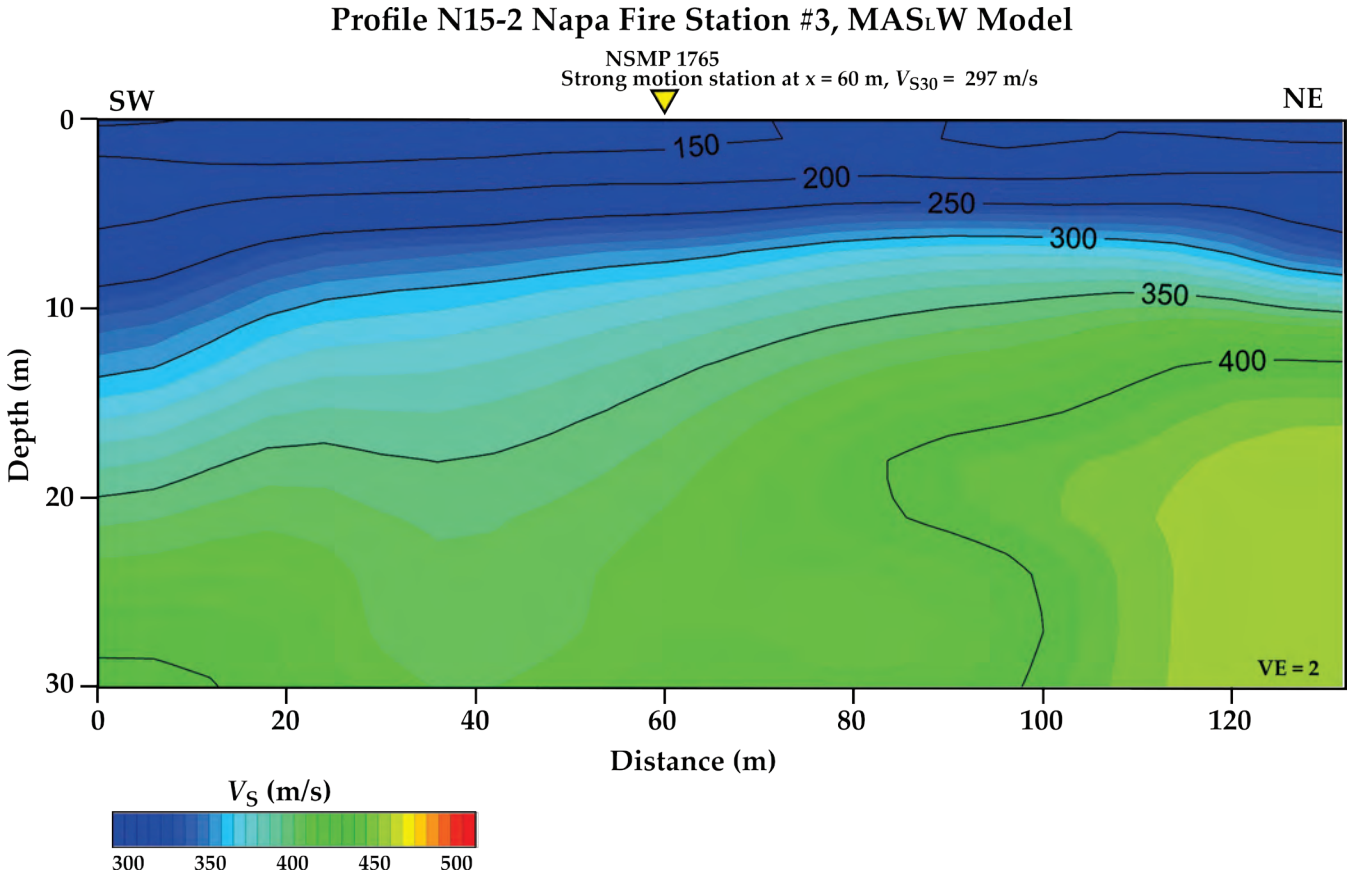

Figure 12. Illustration showing two-dimensional MASLW (multichannel analysis of surface waves for Love waves) shear-wave-velocity model for profile N15-2 at Napa Fire Station Number 3 in Napa, California. S-wave velocities range from 150 meters per second (m/s) at the near surface to about 400 m/s at approximately 20 meters (m) depth. The leaking water tank is located at distance meter 80 along the profile. Strong-motion recording station is nearest to distance meter 60 of our seismic profile. NSMP, National Strong Motion Project; NW, northwest; SE, southeast; VE, vertical exaggeration; $V_{s,}$ shear-wave velocity; V_{S30}, time-averaged shear-wave velocity in the upper 30 meters of the subsurface.

MASRW 2D S-wave Velocity Model

The Rayleigh wave dispersion curves (appendix 1, left column), which represent the location (meter 60) on our seismic profile nearest to the strong-motion recording station, show adjusted picks (red circles) for the fundamental mode at phase velocities between 200 to 300 m/s and at frequencies between 3 to 22 Hz. The fundamental modes are distinct from higher modes in the dispersion curves. Rayleigh wave dispersion curve picks across the entire length of the profile (appendix 2, red triangles) vary between the number of shots used during CMPCC construction (all shots along the profile versus two end shots) and at each single shot gather along the profile. Table 3 and figures in appendix 3 show V_{S30} and 1D velocity-depth results near the strong-motion station; the results come from using varying

MASRW methods—2D MASRW (all shots), 2D MASRW (two end shots), and at shot gather located at distance meter 60.

Along the Napa Fire Station Number 3 seismic profile, V_S ranges from 200 m/s in the near surface to about 340 m/s at 20 m depth (fig. 13). Generally, V_S is slightly lower near the central (meters 70 to 90) part of the seismic profile and higher toward southwestern end of the profile. The shallow-depth velocities compare reasonably well between the MASRW-determined model and the S-wave tomography model.

We calculated V_{S30} nearest to the strong-motion station at meter 60 along the profile. V_{S30} calculated from 2D MASRW analysis using all shot gathers along the profile is 301 m/s. V_{S30} from 2D MASRW analysis using two end shots is 273 m/s. Finally, V_{S30} at a single shot gather nearest to the strong-motion station is 291 m/s.

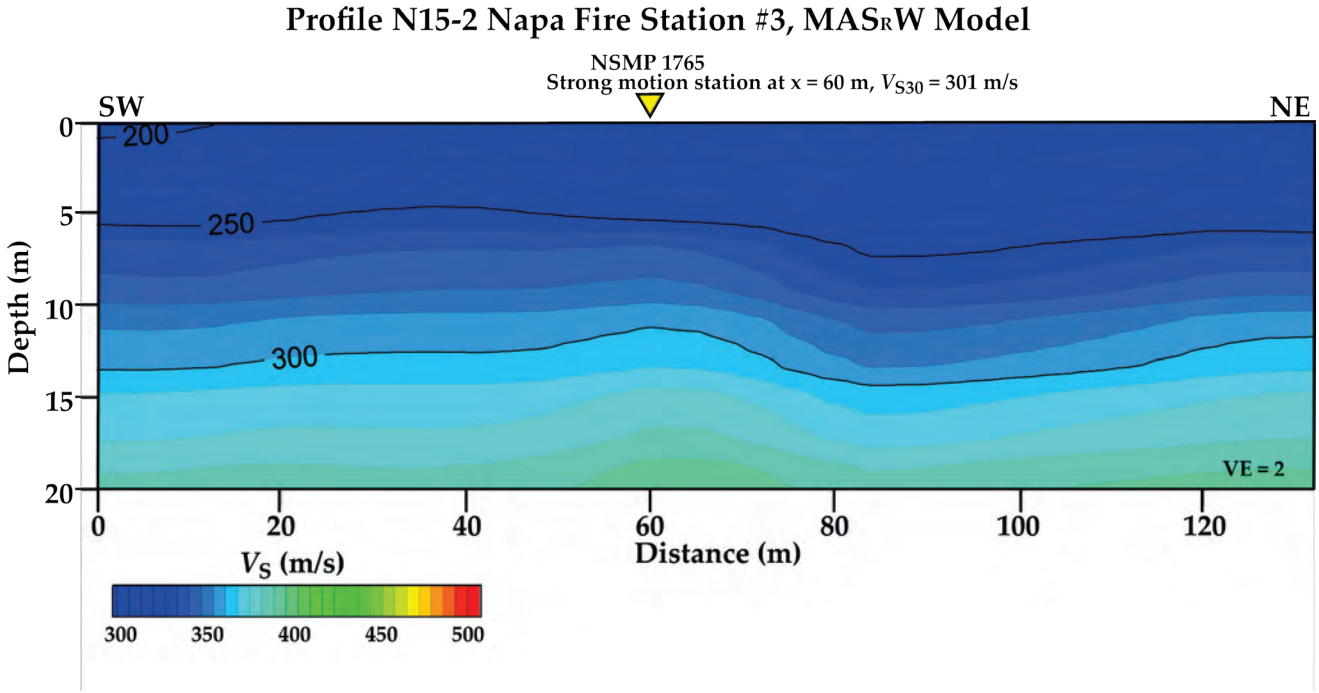

Figure 13. Illustration showing two-dimensional MASRW (multichannel analysis of surface waves for Rayleigh waves) shear-wave velocity model for profile N15-2 at Napa Fire Station Number 3 in Napa, California. S-wave velocities range from 200 meters per second (m/s) at the near surface to about 340 m/s at approximately 20 meters (m) depth. The concave structure coincides with the location of the leaking water tank at distance meter 80. Strong-motion recording station is nearest to distance meter 60 of our seismic profile. NSMP, National Strong Motion Project; NW, northwest; SE, southeast; VE, vertical exaggeration; V_S, shear-wave velocity; V_{S30}, time-averaged shear-wave velocity in the upper 30 meters of the subsurface.

Profile N15-3—Kreuzer Lane (KRE)

P-wave Tomography (V_P) Model

Along our seismic profile at Kreuzer Lane, P-wave velocities range from 800 m/s in the near surface to about 2,700 m/s at about 60 m depth (fig. 14). Unlike along profiles N15-1 and N15-2, topography is more variable along profile N15-3, and velocities are more laterally variable in the shallow subsurface. The 1,500 m/s velocity contour (top of groundwater) varies between about 8 and 20 m beneath the surface.

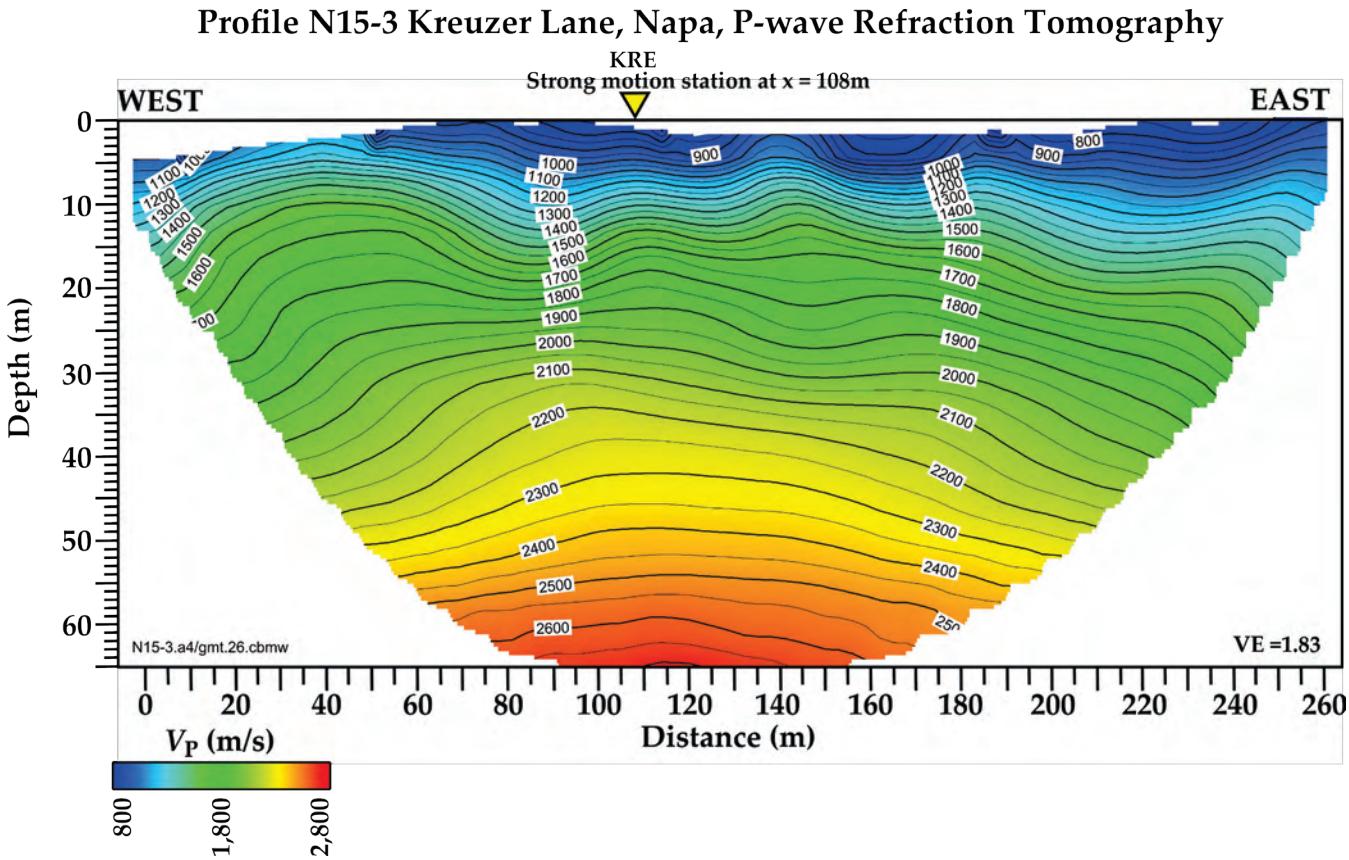

Figure 14. Illustration showing P-wave refraction tomography model for profile N15-3 at Kreuzer Lane (KRE) in Napa County, California. P-wave velocities range from 900 meters per second (m/s) in the near surface to about 2,700 m/s at approximately 65 meters (m) depth. The location of the seismic profile is more than 3 kilometers from the current position of the Napa River and up to 40 m above it. Strong-motion recording station is nearest to distance meter 108 of our seismic profile. V_P, P-wave velocity.

S-wave Tomography (V_S) Model

V_S determined from tomography ranges from 600 m/s in the near surface to about 1,300 m/s at ~60 m depth (fig. 15). The lowest velocities in the near surface coincide with both the topographically lowest and highest points along the seismic profile. The highest velocities are observed in the bottom 10 m of the velocity model, with slightly higher velocities at depth to the east.

Data coverage reached at least 30 m depth between distance meter 21 to meter 228 of the tomography model. The point along the seismic profile closest to the strong-motion recording station was meter 108, where we calculated V_{S30} to be 916 m/s.

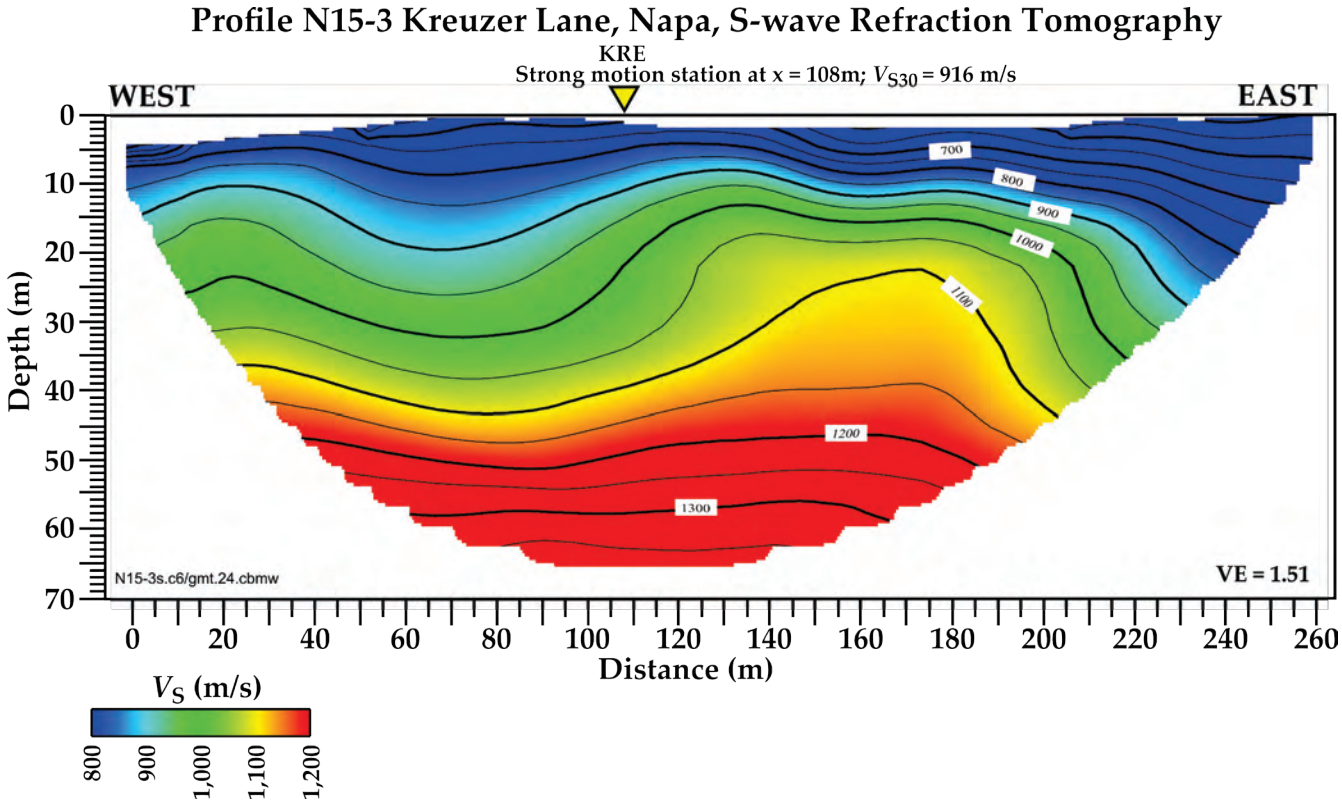

Figure 15. Illustration showing S-wave refraction tomography model for profile N15-3 at Kreuzer Lane (KRE) in Napa County, California. S-wave velocities range from 600 meters per second (m/s) at the near surface to about 1,300 m/s at approximately 60 meters (m) depth. In general, velocities increase slightly to the east below 20 m depth, which is consistent with the local topography and geology. Strong-motion recording station is nearest to distance meter 108 of our seismic profile. V_S, shear-wave velocity; V_{S30}, time-averaged shear-wave velocity in the upper 30 meters of the subsurface.

MASLW 2D S-wave Velocity Model

The Love wave dispersion curves (appendix 1, right column), which represent the location (meter 108) on our seismic profile nearest to the strong-motion recording station, show adjusted picks (red circles) for the fundamental mode at phase velocities between 700 to 1,000 m/s and at frequencies between 10 to 30 Hz. Love wave dispersion curve picks across the entire length of the profile (appendix 2, blue circles) vary between the number of shots used during CMPCC construction (all shots along the profile versus two end shots) and at each single shot gather along the profile. Table 3 and figures in appendix 3 show V_{S30} and 1D velocity-depth results near the strong-motion station; the results come from using varying MASLW methods—2D MASLW (all shots), 2D MASLW (end shots), and at shot gather located at distance meter 108.

Along the Kreuzer Lane seismic profile, 1D MASLW-determined V_S ranges from 600 m/s in the near surface to about 1000 m/s at 30 m depth (fig. 16). Maximum values of V_S in the MASLW and S-wave tomography models differ by about 100 m/s at about 30 m depth, with lower velocities observed in the MASLW model. Similar V_S is observed at the surface between MASLW and S-wave tomography models.

We calculated V_{S30} nearest to the strong-motion station at meter 108 along the profile. V_{S30} calculated from 2D MASLW analysis using all shot gathers along the profile is 885 m/s. V_{S30} from 2D

MASLW analysis using two end shots is 914 m/s. Finally, V_{S30} at a single shot gather nearest to the strong-motion station is 787 m/s.

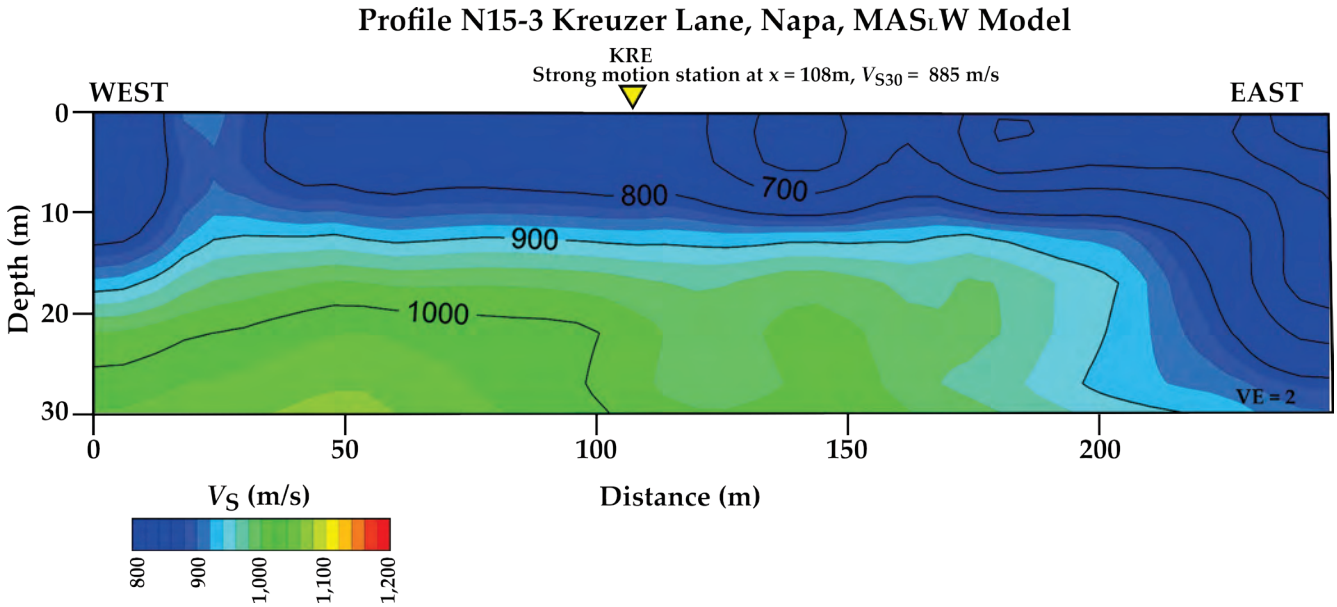

Figure 16. Illustration showing two-dimensional MASLW (multichannel analysis of surface waves for Love waves) shear-wave velocity model for profile N15-3 at Kreuzer Lane (KRE) in Napa County, California. S-wave velocities range from 600 meters per second (m/s) at the near surface to more than 1000 m/s below 20 meters (m) depth. Strong-motion recording station is nearest to distance meter 108 of our seismic profile. V_S, shear-wave velocity; V_{S30}, time-averaged shear-wave velocity in the upper 30 meters of the subsurface.

MASRW 2D S-wave Velocity Model

The Rayleigh wave dispersion curves (appendix 1, left column), which represent the location (meter 108) on our seismic profile nearest to the strong-motion recording station, show adjusted picks (red circles) for the fundamental mode at phase velocities between 500 to 800 m/s and at frequencies between 5 to 36 Hz. Higher modes are observed at higher frequencies and at higher phase velocities. Rayleigh wave dispersion curve picks across the entire length of the profile (appendix 2, red triangles) vary between the number of shots used during CMPCC construction (all shots along the profile versus two end shots) and at each single shot gather along the profile. Table 3 and figures in appendix 3 show V_{S30} and 1D velocity-depth models near the strong-motion station; the results come from using varying MASRW methods—2D MASRW (all shots), 2D MASRW (end shots), and at shot gather located at distance meter 110.

Along the Kreuzer Lane seismic profile, V_S ranges from 400 m/s near the surface at the western end of the profile to about 830 m/s at 35 m depth (fig. 17). Strong lateral variations in velocities are not observed below 10 m depth, except near the bottom (~25 m) of the model, where higher velocities are observed at shallower depths toward the east. Generally, we observe V_S to be significantly lower in the MASRW models relative to S-wave refraction tomography and MASLW models along the Kreuzer Lane profile, likely owing to the variations in topography and subsurface structure, which make MASRW velocity estimation more difficult.

We calculated V_{S30} nearest to the strong-motion station at meter 108 along the profile. V_{S30} calculated from 2D MASRW analysis using all shot gathers along the profile is 695 m/s. V_{S30} from 2D

MASRW analysis using two end shots is 690 m/s. Finally, V_{S30} at a single shot gather nearest to the strong-motion station is 606 m/s.

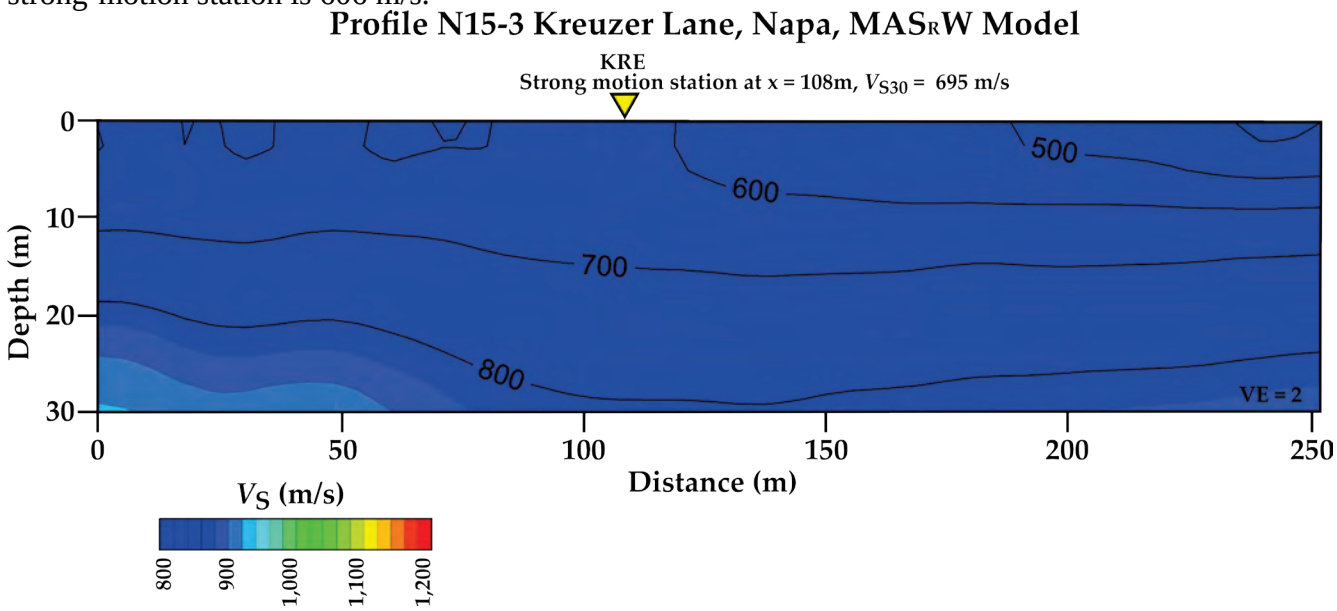

Figure 17. Illustration showing two-dimensional MASRW (multichannel analysis of surface waves for Rayleigh waves) shear-wave velocity model for profile N15-3 at Kreuzer Lane (KRE) in Napa County, California. S-wave velocities range from 500 meters per second (m/s) at the near surface to about 830 m/s at approximately 3 meters (m) depth. Velocity increases slightly to the east, which is consistent with the local topography and geology. Strong-motion recording station is nearest to distance meter 108 of our seismic profile. V_S, shear-wave velocity; V_{S30}, time-averaged shear-wave velocity in the upper 30 meters of the subsurface.

V_P/V_S Ratios

The ratio of P-wave velocities to S-wave velocities (V_P/V_S) can provide additional information about the lithology and the physical state of subsurface materials (Castagna and others, 1985; Tatham, 1982). We derived V_P/V_S models for each of the three seismic profiles presented in this report by dividing the modeled P-wave velocity by the modeled S-wave velocity at each grid of the tomography velocity models. V_P/V_S graphical results are in appendix 4 of this report.

V_P/V_S values along the Downtown Napa seismic profile range from 3 to 5, with the highest values below about 7 m depth. The higher values below 7 m depth are centered between distance meters 50 and 100, and conversely, the lowest V_P/V_S ratios occur at the surface in a narrow zone directly above the highest values. Along the Fire Station Number 3 seismic profile, V_P/V_S ratios range from about 2 to about 6.8; the highest values extend from about 10 m below the surface to the base of the model at about 35 m. The highest V_P/V_S ratios occur at depth in the vicinity of the leaking water tower at distance 80 m, which infers water from the tower had saturated the subsurface at relatively shallow depths. V_P/V_S ratios are highly variable along the Kreuzer Lane seismic profile and range from 1.5 to 2.3. Unlike along the other two profiles presented here, the highest V_P/V_S ratios occur at discrete locations near the surface and at depth in the upper 65 m. The lowest V_P/V_S ratios occur at two discrete locations near the topographically highest part of the seismic profile, which is also nearest to the strong-motion station. The top of groundwater is inferred from P-wave tomography (1,500 m/s velocity contour; fig. 14) to be approximately 10 m below the surface. The near-surface, near-vertical linear features (meters 190 and 210) occur in the vicinity of a culvert that underlies 4th Avenue.

Poisson's Ratios

We developed models of Poisson's ratio directly from the tomographic V_P and V_S models using the calculation determined by Thomsen (1990). Poisson's ratio has been shown in other studies to correlate well with known water saturation levels, determined from boreholes, in the subsurface (Gregory, 1977; Castagna and others, 1985; Catchings and others, 2007). Because liquids have a Poisson's ratio of 0.5, saturated subsurface materials generally have relatively high Poisson's ratios. Poisson's ratio plots are in appendix 5 of this report.

Along the Downtown Napa seismic profile, Poisson's ratios range from 0.43 to 0.48, which are indicative of a high level of water saturation along the entire seismic profile from the very near surface to the base of the model. For example, Catchings and others (2007, 2014) have shown that Poisson's ratios (as determined from tomographic seismic data) in excess of about 0.43 coincide with the known depth to the top of groundwater. Along the Downtown Napa seismic profile, the highest Poisson's ratios occur below 7 m depth near the central part of the seismic profile. Along the Napa Fire Station Number 3 seismic profile, Poisson's ratios near the surface range from 0.30 to 0.49. Poisson's ratios exceed 0.43 (saturation) at depths of about 5 to 8 m along the profile. The highest Poisson's ratio value occurs below12 m depth near distance meter 80, directly below the site of the leaking water tower. Along the Kreuzer Lane seismic profile, Poisson's ratios range from 0.24 to 0.38 and are highly variable along the lateral and vertical extent of the seismic profile. The relatively low Poisson's ratios suggest that there is not a laterally extensive zone of groundwater saturation along the seismic profile in the upper ~65 m. The relatively higher elevations, distance from the Napa River, and drought conditions at the time of our seismic survey may explain the relatively low saturation levels in the shallow subsurface.

Summary

V_S Comparison

Profile N15-1—Main Street Downtown Napa (NCSN N016)

S-wave refraction tomography indicates S-wave velocities range from about 130 to 400 m/s in the upper 30 m, with lateral variation in velocities along the profile in the upper 20 m and becoming more complex from about 20 to 30 m depth. MAS_RW-determined V_S ranges from 210 to 360 m/s in the upper 25 m, with minor lateral variation in velocities in the upper 5 m of the profile. MAS_LW-determined V_S ranges from 170 to 340 m/s in the upper 25 m, with velocities slightly higher in the middle of the profile. S-wave refraction tomography velocities are lower in the upper 5 m of the profile and slightly higher at depths below 20 m in comparison to V_S determined from MAS_RW and MAS_LW. V_S determined from MAS_RW is generally higher in comparison to V_S determined from MAS_LW and S-wave refraction tomography. Both S-wave refraction tomography and MAS_LW models show a concave shape near the center of the profile indicating higher S-wave velocities at shallower depths near the profile center.

V_{S30} calculated near the strong-motion station from the varying $MAS_{R,L}W$ methods and S-wave refraction tomography show results between Love waves and S-wave refraction tomography differ by 2 to 3 percent (table 3); results between Rayleigh waves and S-wave refraction differ by 1 to 11 percent. V_{S30} calculated from Rayleigh waves are generally higher than those calculated from Love waves using 2D $MAS_{R,L}W$ methods (all shots and end shots).

Profile N15-2—Napa Fire Station Number 3 (NSMP 1765)

S-wave refraction tomography indicates S-wave velocities range from 220 to 600 m/s in the upper 45 m. S-wave velocities show significant lateral variation in the upper ~25 m, with a southwest-dipping low-velocity zone at distance meter 80 that coincides with the location of the leaking water tank. V_S determined from MAS$_R$W ranges from 200 to 340 m/s in the upper 20 m; S-wave velocities show slight lateral variation at depths between 5 and 20 m, with a southwest-dipping low-velocity zone beginning at distance meter 70. V_S determined from MAS$_L$W ranges from 150 to 400 m/s in the upper 20 m, with little lateral variation in the upper 8 m but showing more complexity in velocities from 10 to 20 m depth. V_S determined from S-wave refraction tomography is higher at depths below ~5 m, compared to V_S determined from MAS$_R$W and MAS$_L$W. V_S determined from MAS$_R$W is generally higher in the upper ~10 m when compared to V_S determined from MAS$_L$W; however, V_S determined from MAS$_L$W is slightly higher than MAS$_R$W below ~10 m near the center of the profile. Both S-wave refraction tomography and MAS$_R$W models show a southwest-dipping low-velocity zone near distance meter 80 that coincides with the leaking water tower, whereas the MAS$_L$W V_S model does not show the same velocity structure.

V_{S30} calculated near the strong-motion station from the varying MAS$_{R,L}$W methods and S-wave refraction tomography show results between Love waves and S-wave refraction tomography differ by 18 to 22 percent (table 3); results between Rayleigh waves and S-wave refraction differ by 21 to 30 percent. V_{S30} calculated from Love waves are generally higher than those calculated from Rayleigh waves at Napa Fire Station Number 3, with the exception of V_{S30} calculated from 2D MAS$_L$W using all shots along the profile.

Profile N15-3—Kreuzer Lane (KRE)

S-wave refraction tomography shows S-wave velocities range from 600 to 1,300 m/s in the upper 65 m, with significant lateral variation in velocities in the upper ~20 m of the profile. V_S determined from MAS$_R$W ranges from 400 to 830 m/s in the upper 35 m, with complex velocity structures in the upper ~8 m and the lowest velocities at the west end of the profile. V_S determined from MAS$_L$W ranges from 600 to 1,000 m/s in the upper 30 m, with complex velocity structures in the upper 10 m and lowest velocities at the east end of the profile. V_S determined from S-wave refraction tomography is generally higher than MAS$_R$W and MAS$_L$W. V_S determined from MAS$_R$W and MAS$_L$W is similar in the upper ~10 m, with both showing complex lateral variation in velocities. The complex velocity structures continue at depth for MAS$_L$W, and V_S is higher than MAS$_R$W at depths below ~10 m. All three V_S models show a concave shape centered near distance meter 50 at ~8 m depth, but only the S-wave refraction tomography and MAS$_L$W models show the concave velocity structure centered near distance meter 150 at ~20 m depth. Complex velocity structures are apparent in both S-wave refraction tomography and MAS$_L$W models, whereas they are more subdued in the MAS$_R$W model.

V_{S30} calculated near the strong-motion station from the varying MAS$_{R,L}$W methods and S-wave refraction tomography show results between Love waves and S-wave refraction tomography differ by less than 1 percent to 15 percent (table 3); results between Rayleigh waves and S-wave refraction differ by 27 to 41 percent. V_{S30} calculated from Love waves are generally higher than those calculated from Rayleigh waves for Kreuzer Lane.

Conclusion

Our results show that V_S determined from both MAS$_R$W and MAS$_L$W at Napa Fire Station Number 3 and at Kreuzer Lane tended to be lower than V_S determined from S-wave refraction

tomography in the upper ~10 m, and in general, V_S determined from refraction tomography is higher than those determined from MAS_RW and MAS_LW at depths below ~10 m. V_S determined from MAS_LW also tended to be slightly lower than those determined from MAS_RW in the upper ~5 m. However, V_S determined from MAS_LW is generally higher than MAS_RW at depth, with the exception of Main Street in downtown Napa, where V_S determined from MAS_LW is lower than MAS_RW. In general, we found V_S determined from MAS_LW is closer to those determined from S-wave refraction tomography.

V_{S30} calculated from $MAS_{R,L}W$ methods tended to be lower than those calculated from S-wave refraction tomography. Comparison between the varying $MAS_{R,L}W$ methods suggest 2D MAS_LW models using all shot gathers along a profile generally have closer V_{S30} values to those calculated from S-wave refraction tomography.

References Cited

Atwater, T., and Stock, J.M., 2010, Pacific-North America plate tectonics of the Neogene southwestern United States—An update: International Geology Review, v. 40, p. 375–402.

Baltay, A.S., and Boatwright, J., 2015, Ground-motion observations of the 2014 south Napa earthquake: Seismological Research Letters, v. 86, no. 2A, p. 355–360.

Boatwright, J., Blair, J.L., Aagaard, B.T., Wallis, K., 2015, The distribution of red and yellow tags in the city of Napa: Seismological Research Letters, v. 86, no. 2A, p. 361–368.

Boore, D.M., Thompson, E.M., and Cadet, H., 2011, Regional correlations of V_{S30} and velocities averaged over depths less than and greater than 30 meters: Bulletin of the Seismological Society of America, v. 101, no. 6, p 3046–3059.

Brocher, T.M., Baltay, A.S., Hardebeck, J.L., Pollitz, F.F., Murray, J.R., Llenos, A.L., Schwartz, D.P., Blair, J.L., Ponti, D.J., Lienkaemper, J.J., Langenheim, V.E., Dawson, T.E., Hudnut, K.W., Shelly, D.R., Dreger, D.S., Boatwright, J., Aagaard, B.T., Wald, D.J., Allen, R.M., Barnhart, W.D., Knudsen, K.L., Brooks, B.A., and Scharer, K.M., 2015, The M_w 6.0 24 August 2014 south Napa earthquake: Seismological Research Letters, v. 86, no. 2A, p. 309–326.

Building Seismic Safety Council, 2003, Recommended provisions for seismic regulations for new buildings and other structures, part 1—Provisions: Washington, D.C., Federal Emergency Management Agency, Report No. FEMA-450, 303 p.

Castagna, J.P., Batzle, M.L., and Eastwood, R.L., 1985, Relationships between compressional-wave and shear-wave velocities in clastic silicate rocks: Geophysics, v. 50, no. 4, 571–581.

Catchings, R.D., Gandhok, G., Goldman, M.R., Okaya, D., 2001, Seismic images and fault relations of the Santa Monica Thrust Fault, West Los Angeles, California: U.S. Geological Survey Open-File Report 01–111, 34 p., https://pubs.usgs.gov/of/2001/0111/.

Catchings, R.D., Borchers, J.W., Goldman, M.R., Gandhok, G., Ponce, D.A., and Steedman, C.E., 2006, Subsurface structure of the East Bay plain ground-water basin: San Francisco Bay to the Hayward Fault, Alameda County, California: U.S. Geological Survey Open-File Report 2006–1084, 61 p., https://pubs.usgs.gov/of/2006/1084/.

Catchings, R.D., Goldman, M.R., and Gandhok, G., 2007, Structure and velocities of the northeastern Santa Cruz Mountains and the western Santa Clara Valley, California, from seismic imaging: U.S. Geological Survey Open-File Report 2007–1039, 70 p., https://pubs.usgs.gov/of/2007/1039/.

Catchings, R.D., Rymer, M.J., Goldman, M.R., Prentice, C.S., and Sickler, R.R., 2013, Fine-scale delineation of the location of and relative ground shaking within the San Andreas Fault zone at San Andreas Lake, San Mateo County, California: U.S. Geological Survey Open-File Report 2013–1041, 53 p., https://pubs.usgs.gov/of/2013/1041/.

Catchings, R.R., Rymer, M.J., Goldman, M.R., Sickler, R.R., and Criley, C.J., 2014, A method and example of seismically imaging near-surface fault zones in geologically complex areas using V_P, V_S, and their ratios: Bulletin of the Seismological Society of America, v. 104, p. 1989–2006.

Catchings, R.D., Goldman, M.R., Li, Y.-G., and Chan, J.H., 2016, Continuity of the West Napa-Franklin Fault Zone inferred from guided waves generated by earthquake following the 24 August 2014 M_w 6.0 South Napa earthquake: Bulletin of the Seismological Society of America, v. 106, 2721–2746, https://doi.org/10.1785/0120160154.

Catchings, R.D., Goldman, M.R., Trench, David, Buga, Michael, Chan, J.H., Criley, C.J., and Strayer, L.M., 2017a, Shallow-depth location and geometry of the Piedmont Reverse splay of the Hayward Fault, Oakland, California: U.S. Geological Survey Open-File Report 2016–1123, 22 p., https://pubs.usgs.gov/of/2016/1123/.

Catchings, R.D., Goldman, M.R., Chan, J.H., Sickler, R.R., Strayer, L.M., Boatwright, J., and Criley, C.J., 2017b, Basin-wide V_P, V_S, V_P/V_S, and Poisson's ratios of the Napa Valley, California: Seismological Society of America 2017 Annual Meeting Announcement and Program, Seismological Research Letters, v. 88, no. 2B, p. 463–723, https://doi.org/10.1785/0220170035.

Catchings, R.D., Goldman, M.R., and Chan, J.H., 2018, Lateral variations in V_{S30} at six sites near Napa, California: Seismology of the Americas Annual Meeting, Miami, 2018, Seismological Research Letters, v. 89, no. 2B, p. 717–966, https://doi.org/10.1785/0220180082.

Center for Engineering Strong Motion Data, 2017, Peak ground motion data: Center for Engineering Strong Motion Data web page, accessed April 2017 at http://strongmotioncenter.org/cgi-bin/CESMD/apktable.pl?iqrid=SouthNapa_24Aug2014_72282711.

Chan, J.H., Catchings, R.D., Goldman, M.R., and Criley, C.J., 2018, V_{S30} at three strong-motion recording stations in Napa and Solano Counties, California—Lovall Valley Road, Broadway Street and Sereno Drive in Vallejo, and Vallejo Fire Station: U.S. Geological Survey Open-File Report 2018–1162, 62 p., https://doi.org/10.3133/ofr20181162.

DeLong, S.B., Lienkaemper, J.J., Pickering, A.J., and Avdievitch, N.N., 2015, Rates and patterns of surface deformation from laser scanning following the South Napa earthquake, California: Geosphere, v. 11, no. 6, p. 2015–2030., https://doi.org/10.1130/GES01189.1.

Fox, K.F., Jr., Sims, J.D., Bartow, J.A., and Helley, E.J., 1973, Preliminary geologic map of eastern Sonoma County and western Napa County, California: U.S. Geological Survey Miscellaneous Field Studies Map MF 483, scale 1:62,500. [Also available at https://pubs.er.usgs.gov/publication/mf483.]

Fox, K.F., Jr., Fleck, R.J., Curtis, G.H., and Meyer, C.E., 1985a, Implications of the northwesterly younger age of the volcanic rocks of west-central California: Geological Society of America Bulletin, v. 96, p. 647–654.

Fox, K.F. Jr., Fleck, R.J., Curtis, G.H., and Meyer, C.E., 1985b, Potassium-argon and fission-track ages of the Sonoma Volcanics in an area north of San Pablo Bay, California: U.S. Geological Survey Miscellaneous Field Studies Map MF 1753, scale: 1:250,000. [Also available at https://pubs.er.usgs.gov/publication/mf1753.]

Geometrics, Inc., 2016, SeisImager/SW-Pro™ manual—windows software for analysis of surface waves, ver. 1.2: Geometrics, Inc., 74 p.

Goldman, M.R., Catchings, R.D., Chan, J.H., and Criley, C.J., 2018, 2015 high resolution seismic data recorded at six strong motion seismograph sites in Napa and Solano counties, California: U.S. Geological Survey data release, https://doi.org/10.5066/P9F4IAAL.

Graymer, R.W., Sarna-Wojcicki, A.M., Walker, J.P., McLaughlin, R.J., and Fleck, R.J., 2002, Controls on timing and amount of right-lateral displacement on the East Bay fault system, San Francisco Bay region, California: Geological Society of American Bulletin, v. 114, p. 1471–1479.

Graymer, R.W., Bryant, W., McCabe, C.A., Hecker, S., and Prentice, C.S., 2006, Map of Quaternary-active faults in the San Francisco Bay region: U.S. Geological Survey Scientific Investigations Map 2919, https://pubs.usgs.gov/sim/2006/2919.

Graymer, R.W., Brabb, E.E., Jones, D.L., Barnes, J., Nicholson, R.S., and Stamski, R.E., 2007, Geologic map and map database of eastern Sonoma and western Napa Counties, California: U.S. Geological Survey Scientific Investigations Map 2956, https://pubs.usgs.gov/sim/2007/2956/.

Gregory, A.R., 1977, Fluid saturation effects on dynamic elastic properties of sedimentary rocks: Geophysics, v. 41, 895–921.

Hayashi, K., 2003, CMP analysis of multi-channel surface wave data and its application to near-surface S-wave velocity delineation: Symposium on the Application of Geophysics to Engineering and Environmental Problems 2003—Proceedings of the Symposium on the Application of Geophysics to Engineering and Environmental Problems, p. 1348–1355.

Hayashi, K., and Suzuki, H., 2004, CMP cross-correlation analysis of multi-channel surface-wave data: Exploration Geophysics, v. 35, p. 7–13.

Hayashi, K., Cakir, R., and Walsh, T.J., 2016, Comparison of dispersion curves and velocity models obtained by active and passive surface wave methods: Society of Exploration Geophysicist Technical Program Expanded Abstracts 2016, p. 4983–4988, https://doi.org/10.1190/segam2016-13846390.1.

Helley, E.J., and Herd, D.G., 1977, Map showing faults with Quaternary displacement, northeastern San Francisco Bay area region, California: U.S. Geological Survey Miscellaneous Field Studies Map MF–881, scale 1:125,000.

Hole, J.A., 1992, Nonlinear high-resolution three-dimensional seismic travel time tomography: Journal of Geophysical Research, v. 97, no. B5, p. 6553–6562.

Howell, D.G., and Swinchatt, J.P., 2000, A discussion of geology, soils, wines, and history of the Napa Valley region, *in* Lageson, D.R., Peters, S.G., and Lahren, M.M., eds., Great Basin and Sierra Nevada: Boulder, Colorado, Geological Society of America Field Guide 2, p. 415–422.

International Code Council, Inc., 2009, International building code: International Code Council, Inc., 752 p.

Ivanov, J., Miller, R.D., Park, C.P., and Ryden, N., 2003, Seismic search for underground anomalies: Society of Exploration Geophysicists Technical Program Expanded Abstract 2003, p. 1223–1226.

Ivanov, J., Leitner, B., Shefchik, W., Shwenk, J.T., and Peterie, S.L., 2013, Evaluating hazards at salt cavern sites using multichannel analysis of surface waves: The Leading Edge, v. 32, no. 3, p. 298–305.

Knudsen, K.L., Sowers, J.M., Witter, R.C., Wentworth, C.M., and Helley, E.J., 2000, Preliminary maps of Quaternary deposits and liquefaction susceptibility, nine-county San Francisco Bay region, California; a digital database: U.S. Geological Survey Open-File Report 00–444, 2 sheets, scale 1:275,000, https://pubs.usgs.gov/of/2000/of00-444.

Kunkel, F., and Upson, J.E., 1960, Geology and ground water in Napa and Sonoma valleys, Napa and Sonoma Counties, California: U.S. Geological Survey Water-Supply Paper 1495, 252 p., https://pubs.usgs.gov/wsp/1495.

Langenheim, V.E., Graymer, R.W., and Jachens, R.C., 2006, Geophysical settings of the 2000 ML 5.2 Yountville, California, earthquake—Implications for seismic hazard in Napa Valley, California: Bulletin of the Seismological Society of America, v. 96, no. 3, p. 1192–1198.

Langenheim, V.E., Graymer, R.W., Jachens, R.C., McLaughlin, R.J., Wagner, D.L., and Sweetkind, D.S., 2010, Geophysical framework of the northern San Francisco Bay region, California: Geosphere, v. 6, no. 5, p. 594–620.

Li, Y.G., Catchings, R.D., and Goldman, M.R., 2016, Subsurface fault damage zone of the 2014 M_W 6.0 South Napa, California, earthquake viewed form fault-zone trapped waves: Bulletin of the Seismological Society of America, v. 106, no. 6, p. 2747-2763, doi:10.1785/0120160039.

Lienkaemper, J.J., Delong, S.B., Domrose, C.J., and Rosa, C.M., 2016, Afterslip behavior following the 2016 M 6.0 South Napa earthquake with implications for afterslip forecasting on other seismogenic faults: Seismological Research Letters, v. 87, no. 3, p. 609-619, doi:10.1785/0220150262.

Miller, R.D., Xia, J., Park, C.B., and Ivanov, J., 1999, Using MASW to map bedrock in Olathe, Kansas: Kansas Geological Survey Open-File Report No. 99–9, 9 p.

Morelan, A.E., Trexler, C.C., and Oskin, M.E., 2015, Surface-rupture and slip observations on the day of the 24 August 2014 south Napa earthquake: Seismological Research Letters, v. 86, no. 4, p. 1119–1127.

Odum, J.K., Stephenson, W.J., Williams, R.A., and Hillebrandt-Andrade, C., 2013, V_{S30} and spectral response from collocated shallow, active-, and passive-source V_S data at 27 sites in Puerto Rico: Bulletin of the Seismological Society of America, v. 103, no. 5, p. 2709–2728.

Park, C., 2013, MASW for geotechnical site investigation: The Leading Edge, v. 32, no. 6, p.656–662.

Park, C., Miller, R., and Xia, J., 1999, Multichannel analysis of surface waves: Geophysics, v. 64, no. 3, p. 800–808.

Park, C., Miller, R., Xia, J., and Ivanov, J., 2000, Multichannel analysis of surface waves (MASW)—active and passive methods: The Leading Edge, v. 26, p. 60–64, https://doi.org/10.1190/1.2431832.

Pujol, J., 2003, Elastic wave propagation and generation in seismology: Cambridge University Press, United Kingdom, 462 p.

Stonebridge Research Group LLC, 2012, The economic impact of Napa County's wine and grapes: Stonebridge Research Group LLC, accessed March 2017 at https://napavintners.com/community/docs/napa_economic_impact_2012.pdf.

Sweetkind, D.S., Rytuba, J.J., Langenheim, V.E., and Sarna-Wojcicki, A.M., 2005, Contrasting styles of volcanism along the east side of Napa Valley, CA: Geological Society of America Abstracts with Program, v. 37, no. 4, p. 84.

Tatham, R.H., 1982, V_P/V_S and lithology: Geophysics, v. 47, no. 3, p. 336–344.

Thomsen, L., 1990, Poisson was not a geophysicist!: The Leading Edge, v. 9, p. 27–29.

U.S. Census Bureau, 2010, QuickFacts: U.S. Census Bureau web page accessed March 2017 at https://www.census.gov/quickfacts/fact/table/napacitycalifornia,napacountycalifornia/PST045216.

U.S. Geological Survey, 2015, South Napa Earthquake – One Year Later: U.S. Geological Survey page accessed June 2018 at https://www.usgs.gov/news/south-napa-earthquake-%E2%80%93-one-year-later.

Wagner, D.L., Saucedo, G.J., Clahan, K.B., Fleck, R.J., Langenheim, V.E., McLaughlin, R.J., Sarna-Wojcicki, A.M., Allen, J.R., and Deino, A.L., 2011, Geology, geochronology, and paleogeography of the southern Sonoma volcanic field and adjacent areas, northern San Francisco Bay region, California: Geosphere, v. 7, no. 3, p. 658–683.

Weaver, C.E., 1949, Geology of the Coast Ranges immediately north of the San Francisco Bay region, California: Geological Survey of America Memoir 35, 242 p.

Xia, J., Miller, R., Park, C., and Ivanov, J., 2000, Construction of 2 D vertical shear wave velocity field by the multichannel analysis of surface wave technique, *in* Symposium on the Application of Geophysics to Engineering and Environmental Problems 2000: Society of Exploration Geophysicists, Environment and Engineering Geophysical Society, p. 1197–1206, https://doi.org/10.4133/1.2922726.

Yong, A., Martin, A., Stokoe, K., and Diehl, J., 2013, ARRA-funded V_{S30} measurements using multi-technique approach at strong-motion stations in California and Central-Eastern United States: U.S.

Geological Survey Open-File Report 2013–1102, 60 p. and data files, https://pubs.usgs.gov/of/2013/1102/.

Appendix 1—Rayleigh and Love Wave Dispersion Curves

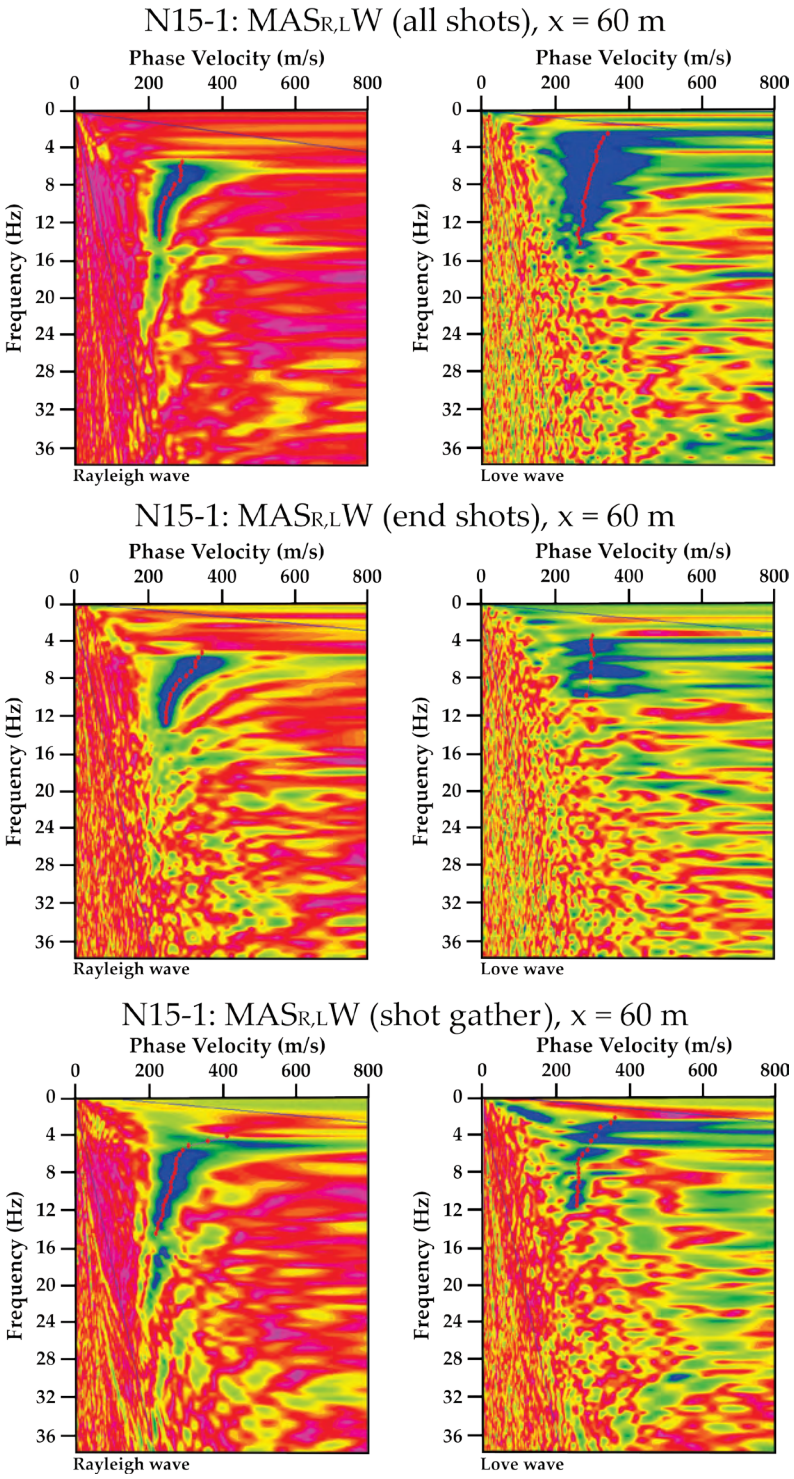

Figure 18. Graphs showing Rayleigh and Love wave dispersion curves representing the point on our seismic profile N15-1: Main Street downtown Napa, California, that is nearest to the strong-motion station. Adjusted picks (red dots) for the fundamental mode are at phase velocities between 200 and 400 meters per second (m/s) and at frequencies between 4 and 15 hertz (Hz). $MAS_{R,L}W$, multichannel analysis of surface waves for both Rayleigh and Love waves.

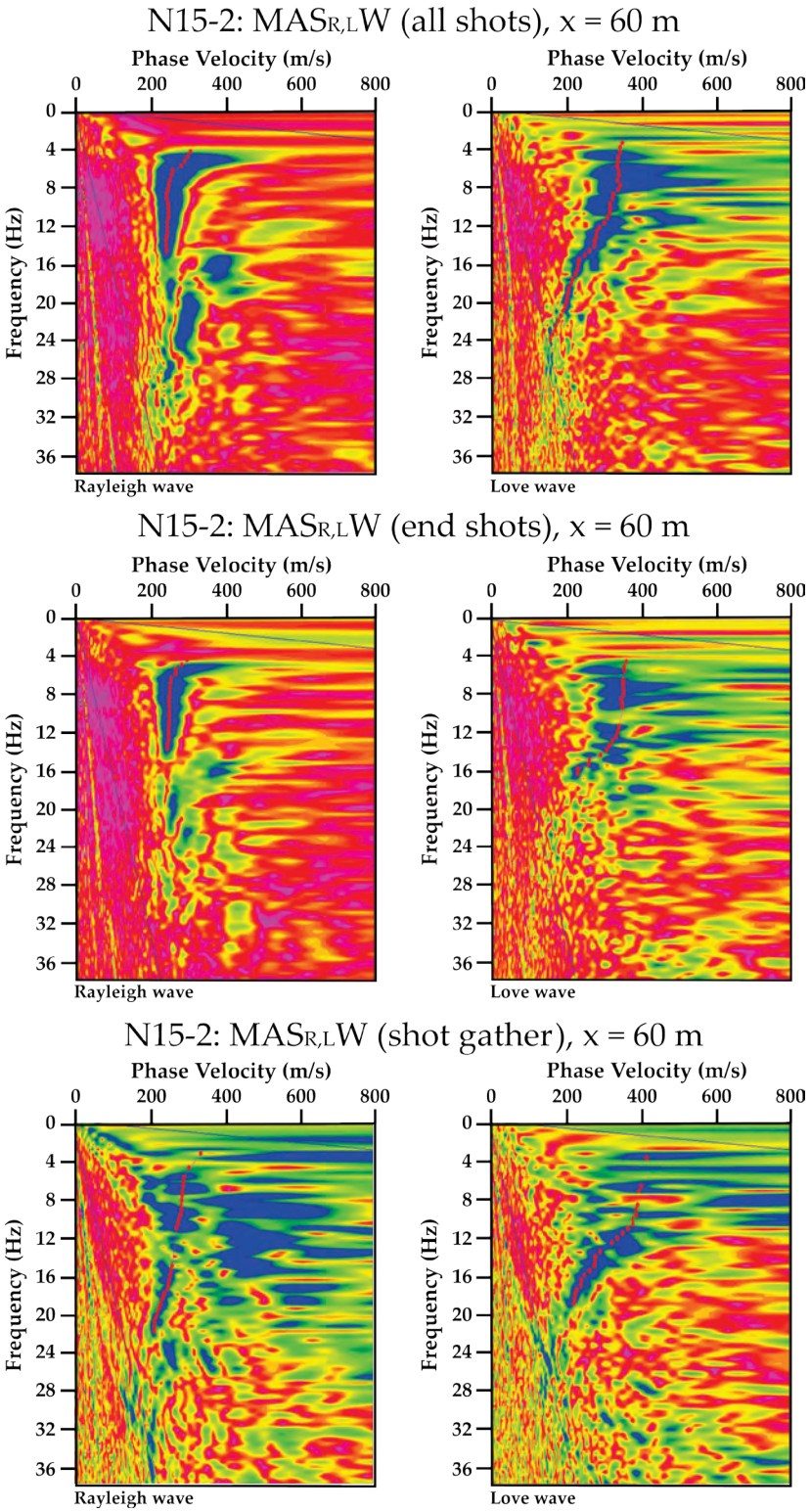

Figure 19. Graphs showing Rayleigh and Love wave dispersion curves representing the point on our seismic profile N15-2: Napa Fire Station Number 3, Napa County, California, that is nearest to the strong-motion station. Adjusted picks (red dots) for the fundamental mode are at phase velocities between 200 and 400 meters per second (m/s) and at frequencies between 3 and 24 hertz (Hz). $MAS_{R,L}W$, multichannel analysis of surface waves for both Rayleigh and Love waves.

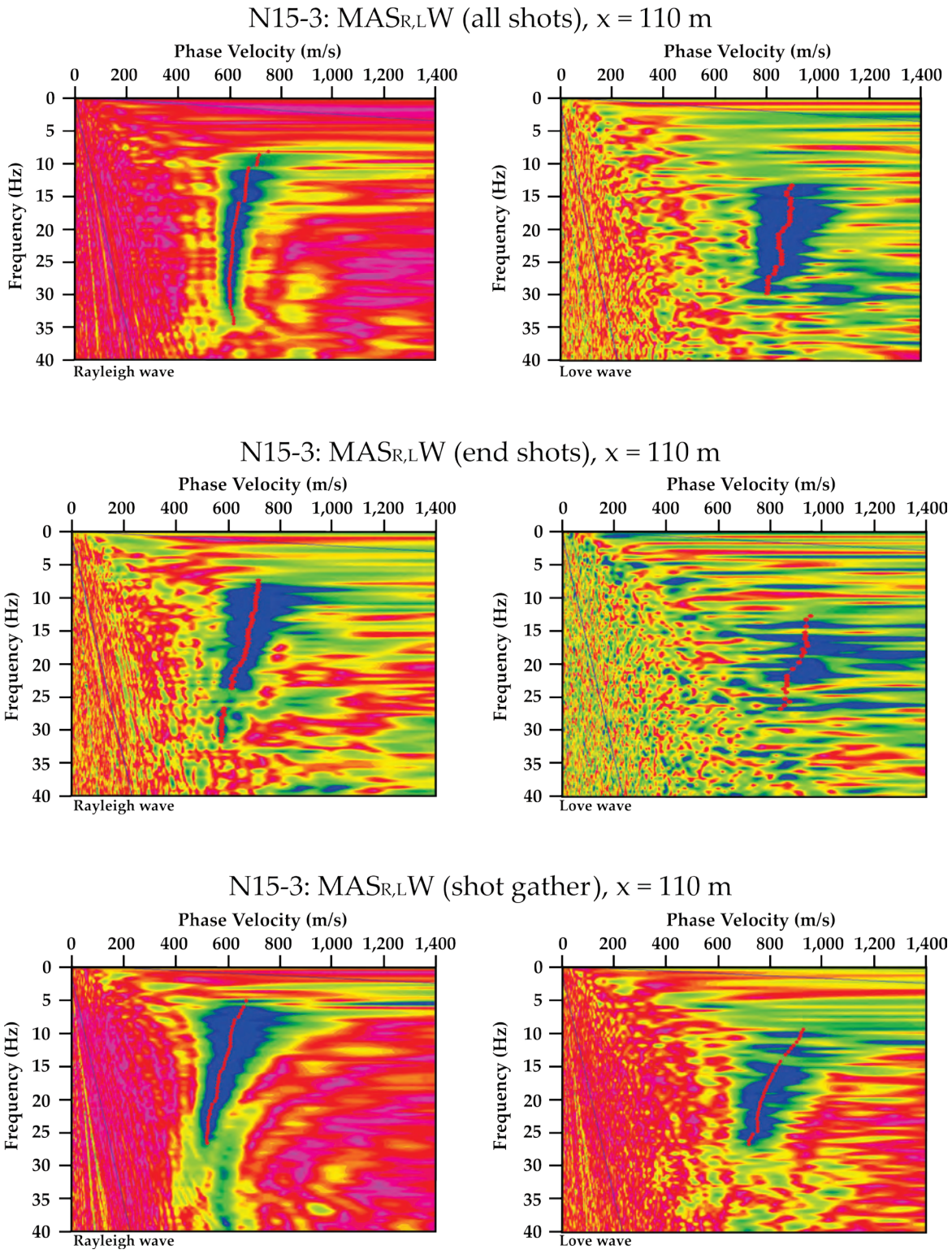

Figure 20. Graphs showing Rayleigh and Love wave dispersion curves representing the point on our seismic profile N15-3: Kreuzer Lane, Napa, California, that is nearest to the strong-motion station. Adjusted picks (red dots) for the fundamental mode are at phase velocities between 550 and 1,000 meters per second (m/s) and at frequencies between 5 and 35 hertz (Hz). MASR,LW, multichannel analysis of surface waves for both Rayleigh and Love waves.

Appendix 2—Rayleigh and Love Wave Fundamental Mode Dispersion Curve Picks

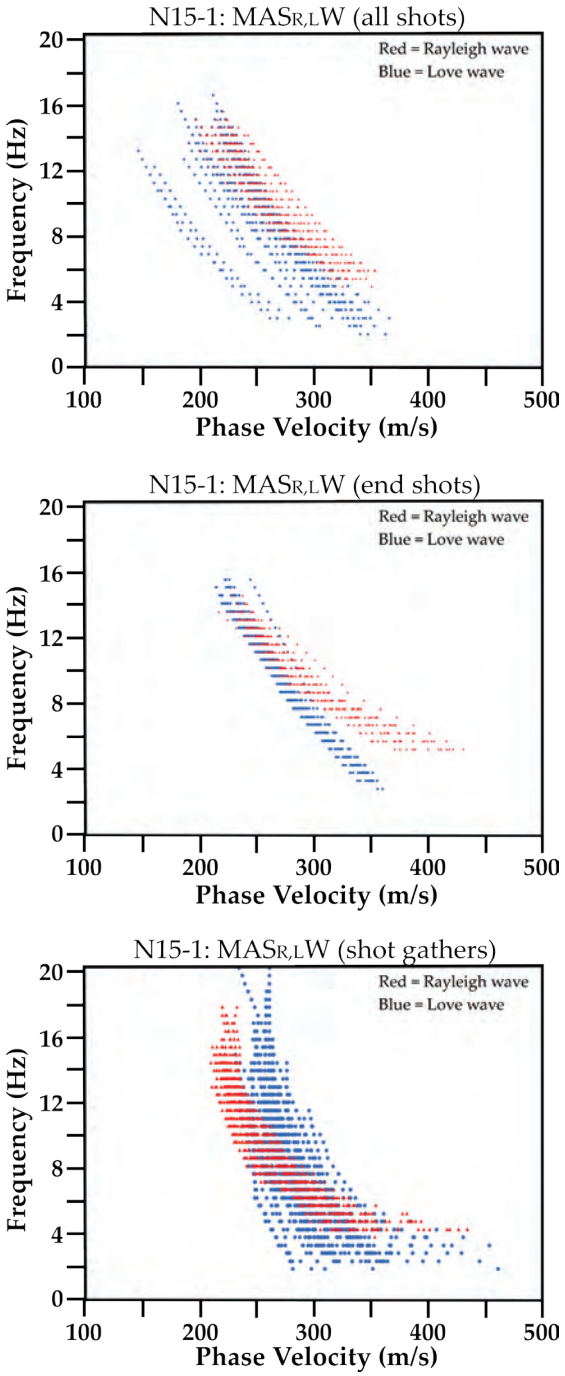

Figure 21. Graphs showing Rayleigh (red dots) and Love (blue dots) wave fundamental mode dispersion curve picks across the entire length of the seismic profile N15-1: Main Street downtown Napa, California; dispersion curve picks vary between the number of shots used during common mid-point cross-correlation (CMPCC) construction (all shots along the profile versus two end shots) and at each single shot gather along the profile. $MAS_{R,L}W$, multichannel analysis of surface waves for both Rayleigh and Love waves. Hz, hertz; m/s, meters per second.

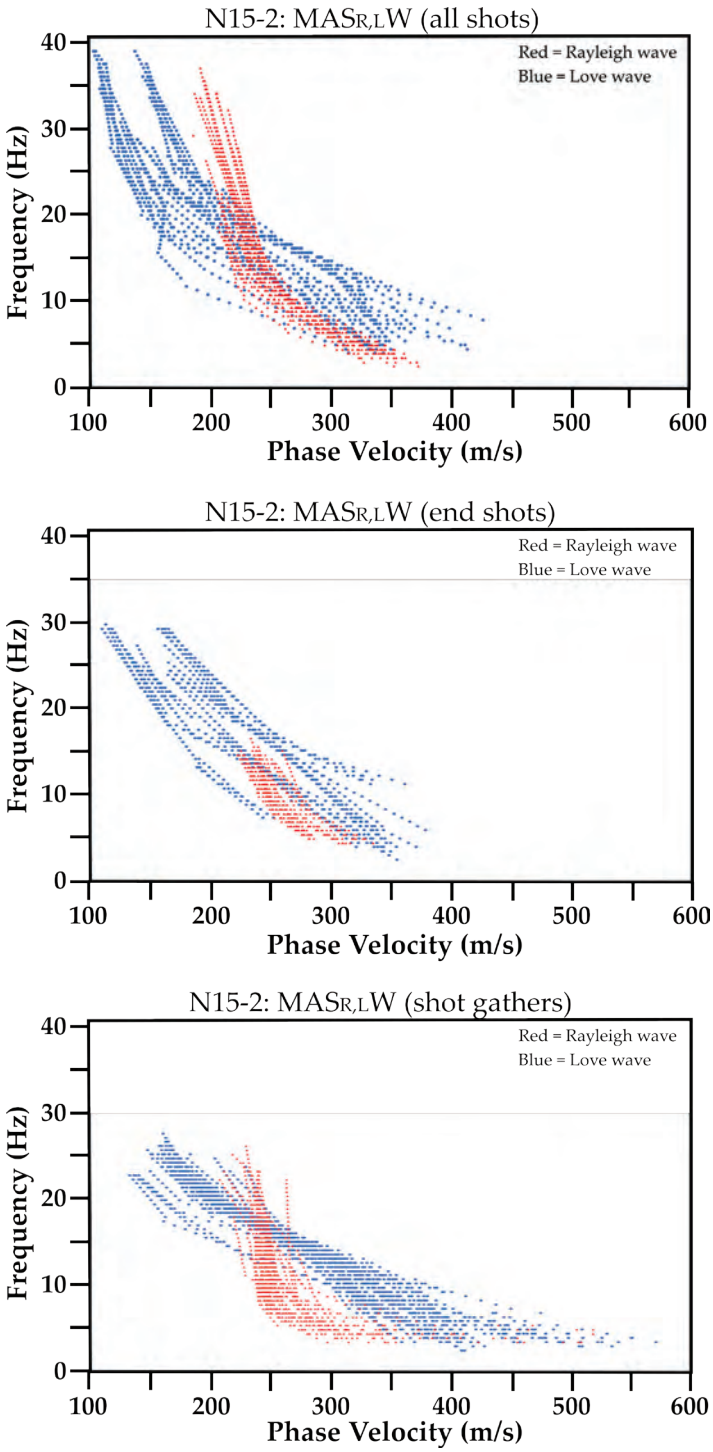

Figure 22. Graphs showing Rayleigh (red dots) and Love (blue dots) wave fundamental mode dispersion curve picks across the entire length of the seismic profile N15-2: Napa Fire Station Number 3, Napa County, California; dispersion curve picks vary between the number of shots used during common mid-point cross-correlation (CMPCC) construction (all shots along the profile versus two end shots) and at each single shot gather along the profile. MASR,LW, multichannel analysis of surface waves for both Rayleigh and Love waves. Hz, hertz; m/s, meters per second.

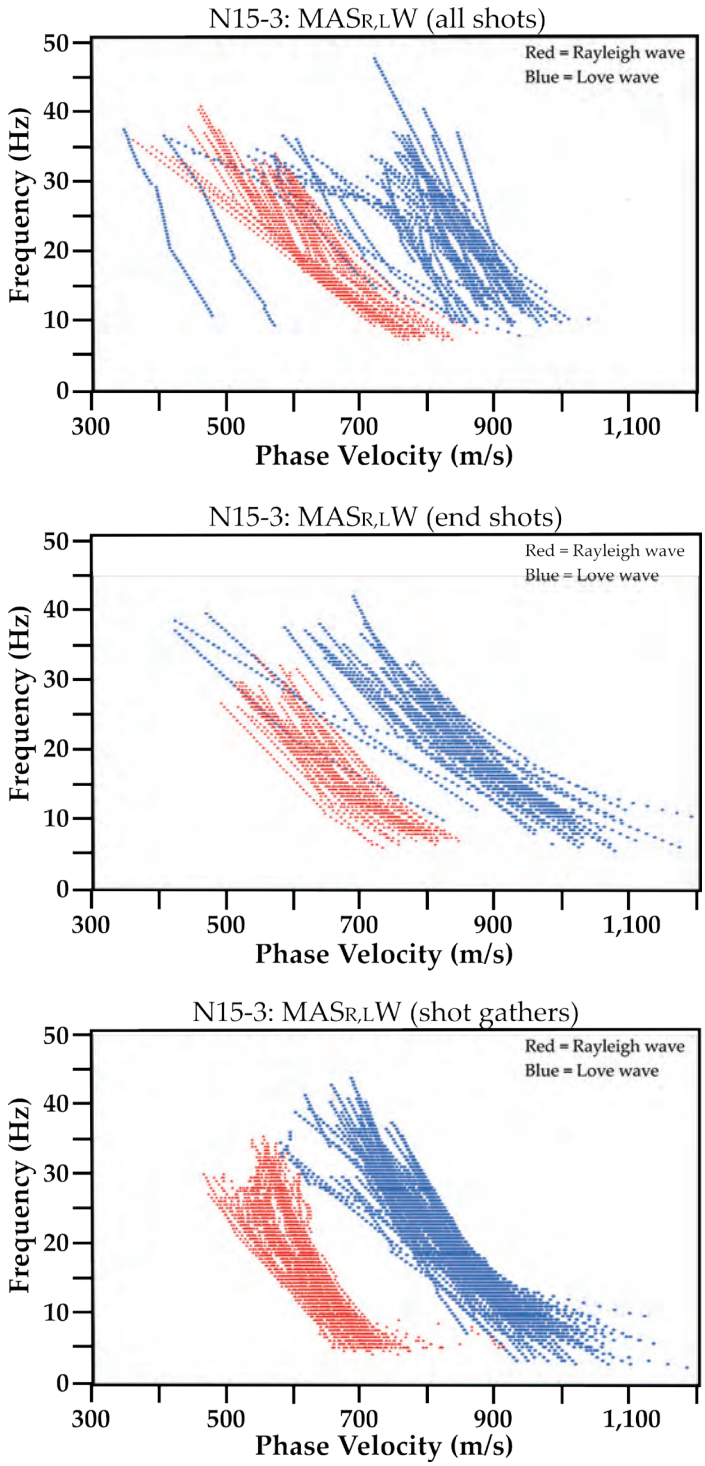

Figure 23. Graphs showing Rayleigh (red dots) and Love (blue dots) wave fundamental mode dispersion curve picks across the entire length of the seismic profile N15-3: Kreuzer Lane, Napa, California; dispersion curve picks vary between the number of shots used during common mid-point cross-correlation (CMPCC) construction (all shots along the profile versus two end shots) and at each single shot gather along the profile. $MAS_{R,L}W$, multichannel analysis of surface waves for both Rayleigh and Love waves. Hz, hertz; m/s, meters per second.

Appendix 3—Rayleigh Wave, Love Wave, and S-Wave Refraction Tomography 1D Velocity-Depth Profiles

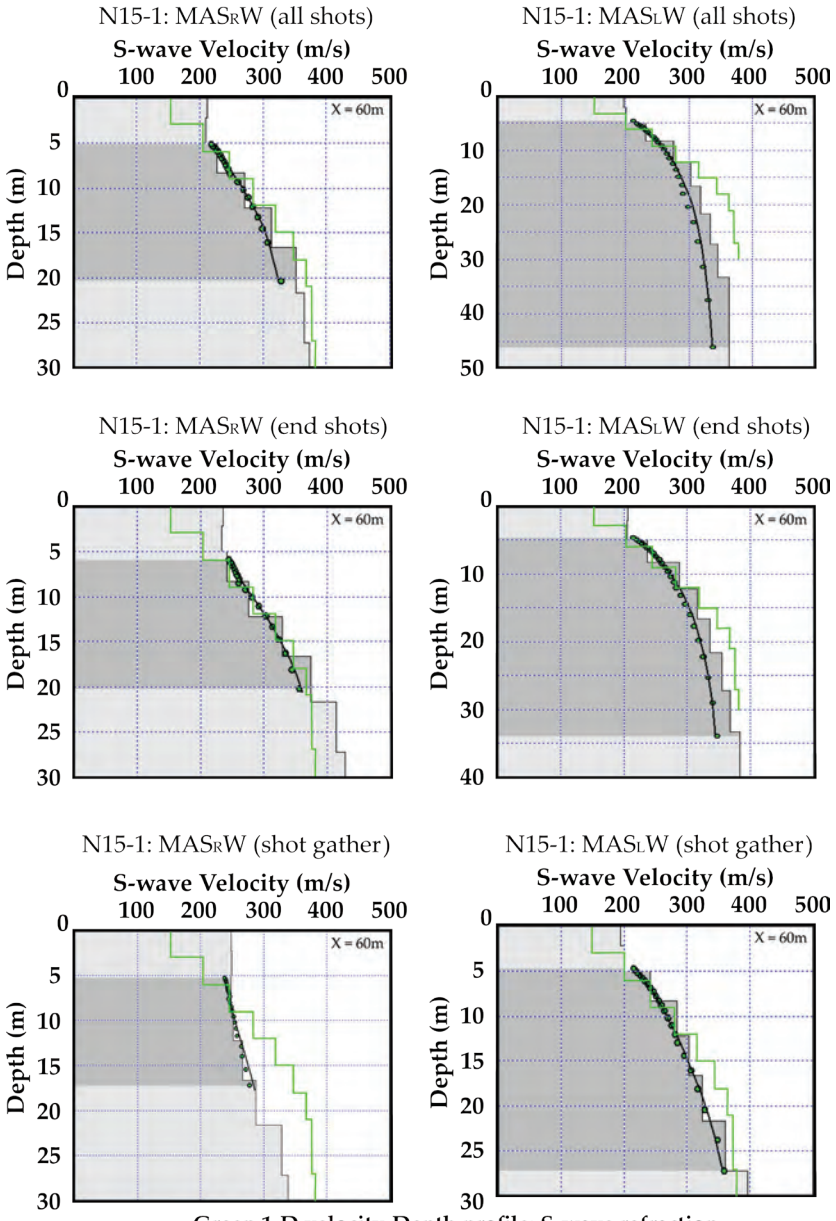

Figure 24. Graphs showing Rayleigh wave (left column), Love wave (right column), and S-wave refraction tomography (green line) one-dimensional (1D) velocity-depth profiles representing the point on our seismic profile N15-1: Main Street downtown Napa, California, that is nearest to the strong-motion station. One-dimensional velocity-depth profiles from multichannel analysis of surface waves (MASW) analysis using both Love and Rayleigh waves generally agree well with those determined from S-wave refraction tomography. Green dots on the 1D velocity-depth profiles are dispersion curve picks, and black lines are the model fit to the picks. MAS_RW, multichannel analysis of surface waves for Rayleigh waves; MAS_LW, multichannel analysis of surface waves for Love waves; m, meters; m/s; meters per second.

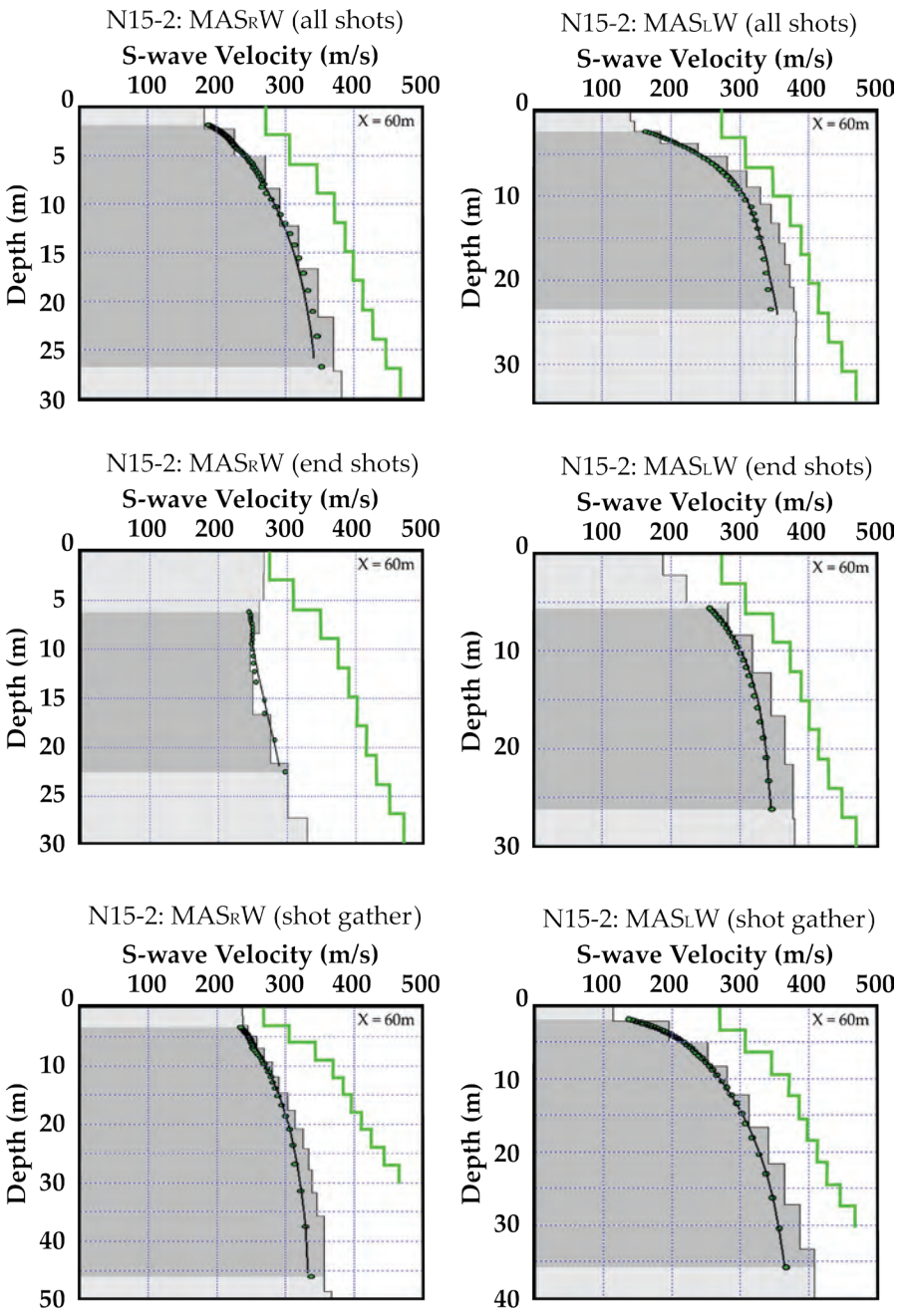

Figure 25. Graphs showing Rayleigh wave (left column), Love wave (right column), and S-wave refraction tomography (green line) one-dimensional (1D) velocity-depth profiles representing the point on our seismic profile N15-2: Napa Fire Station Number 3, Napa, California, that is nearest to the strong-motion station. One-dimensional velocity-depth profiles from multichannel analysis of surface waves (MASW) analysis using both Love and Rayleigh waves generally are slower than those determined from S-wave refraction tomography. Green dots on the 1D velocity-depth profiles are dispersion curve picks, and black lines are the model fit to the picks. MASRW, multichannel analysis of surface waves for Rayleigh waves; MASLW, multichannel analysis of surface waves for Love waves; m, meters; m/s; meters per second.

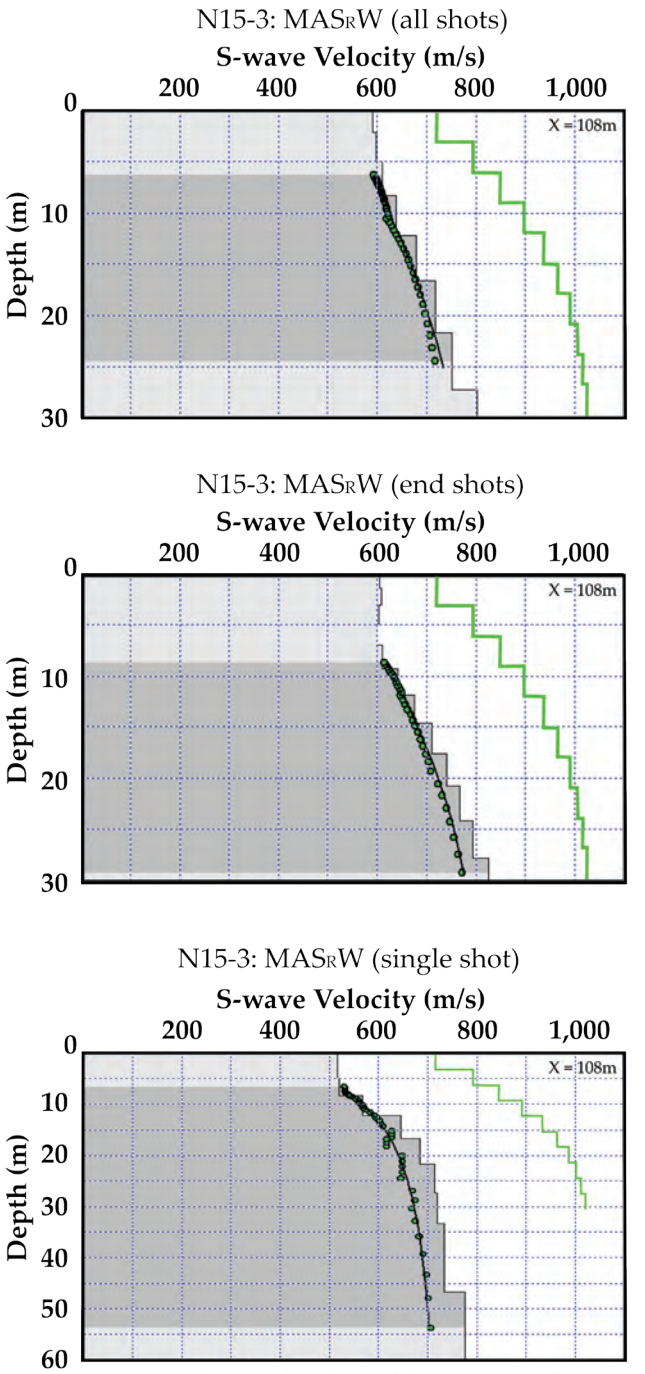

Figure 26. Graphs showing Rayleigh wave and S-wave refraction tomography (green line) one-dimensional (1D) velocity-depth profiles representing the point on our seismic profile N15-3: Kreuzer Lane, Napa County, California, that is nearest to the strong-motion station. One-dimensional velocity-depth profiles from multichannel analysis of surface waves (MASW) analysis using Rayleigh waves generally are slower than those determined from S-wave refraction tomography. Green dots on the 1D velocity-depth profiles are dispersion curve picks, and black lines are the model fit to the picks. MASRW, multichannel analysis of surface waves for Rayleigh waves; m, meters; m/s; meters per second.

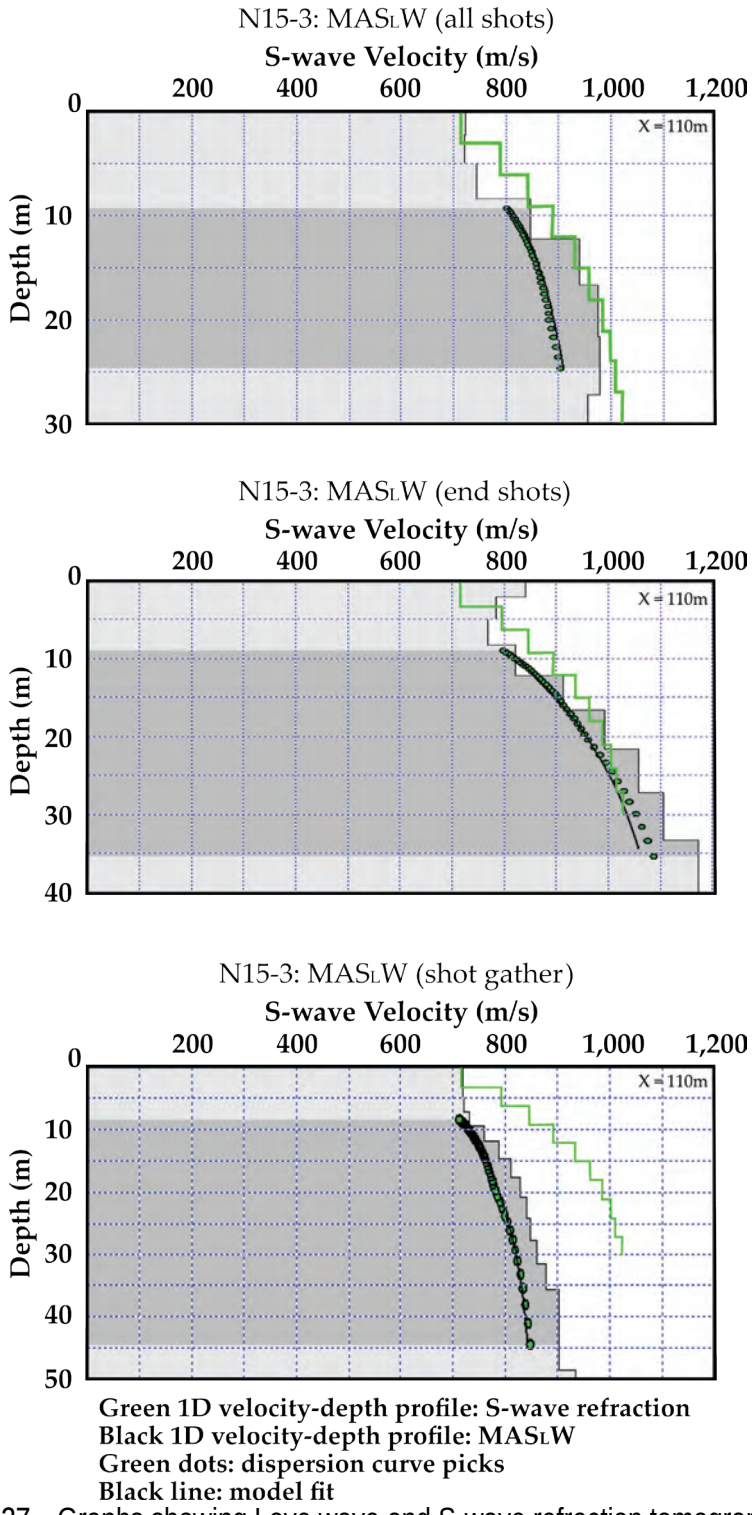

Figure 27. Graphs showing Love wave and S-wave refraction tomography (green line) one-dimensional (1D) velocity-depth profiles representing the point on our seismic profile N15-3: Kreuzer Lane that is nearest to the strong-motion station. One-dimensional velocity-depth profiles from MASW analysis using Love waves are generally similar to those determined from S-wave refraction tomography. Green dots on the 1D velocity-depth profiles are dispersion curve picks, and black lines are the model fit to the picks. MASLW, multichannel analysis of surface waves for Love waves; m, meters; m/s; meters per second.

Appendix 4—V_P/V_S Ratio Determined from P- and S-Wave Refraction Tomography

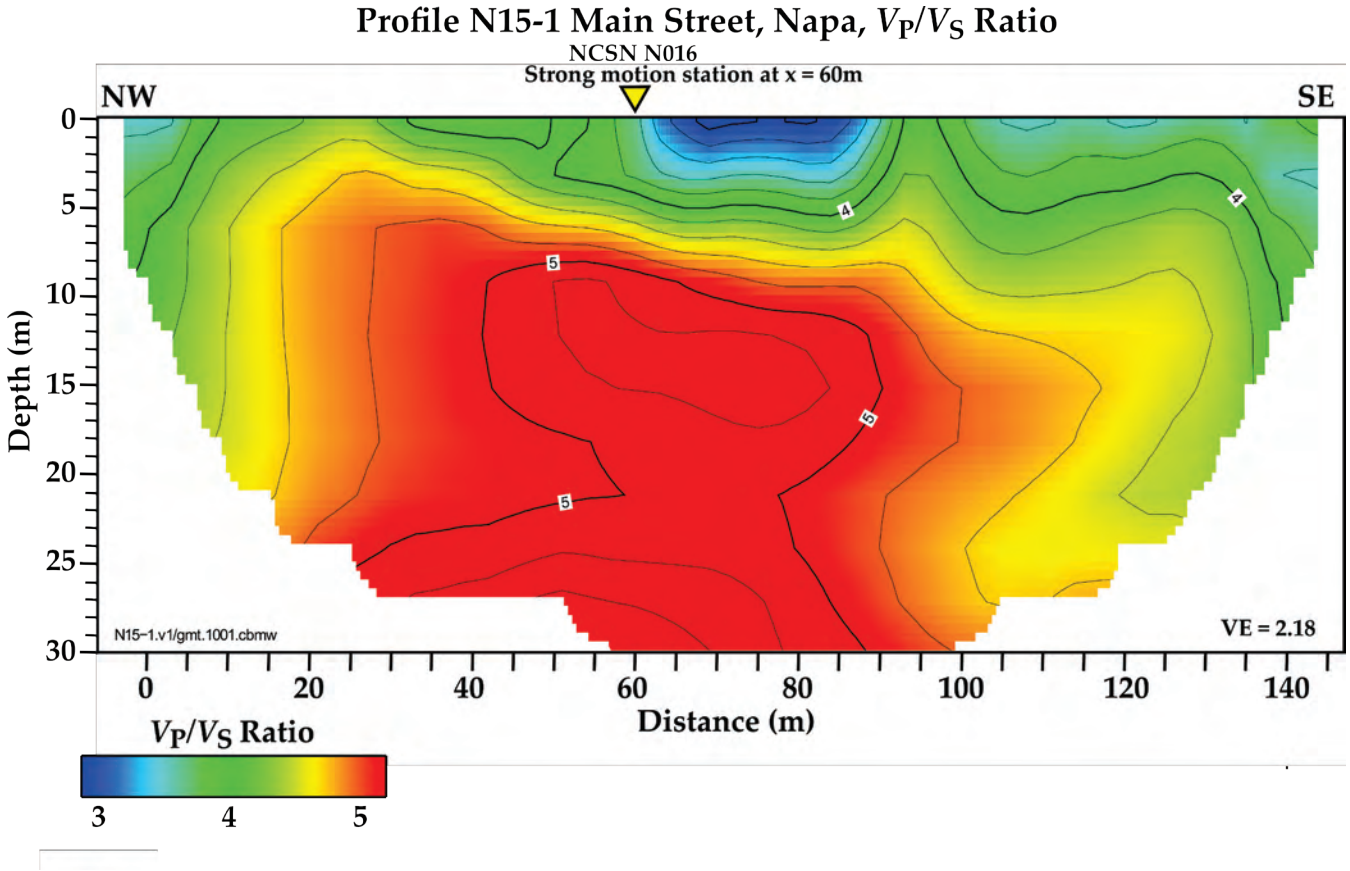

Figure 28. Illustration showing the ratio of P-wave velocity to S-wave velocity (V_P/V_S) determined from P- and S-wave refraction tomography along Main Street in downtown Napa, California, seismic profile range from 3 to 5, with the highest values below 7 meters (m) depth. NCSN, Northern California Seismic Network; NW, northwest; SE, southeast; VE, vertical exaggeration.

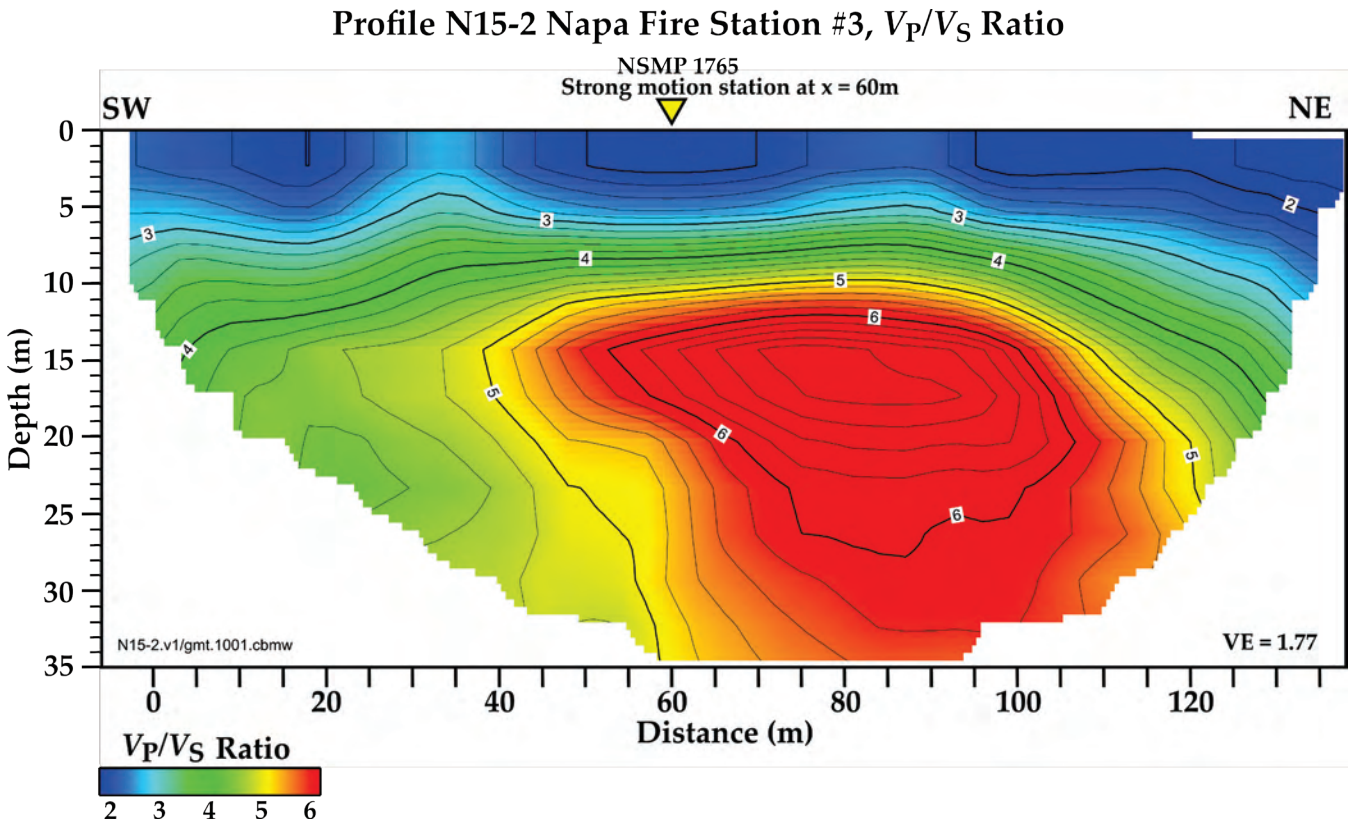

Figure 29. Illustration showing the ratio of P-wave velocity to S-wave velocity (V_P/V_S) determined from P- and S-wave refraction tomography along Napa Fire Station 3, Napa, California, seismic profile range from 2 to 6.8, with the highest values below 10 meters (m) depth. The highest V_P/V_S ratios occur near the leaking water tower at distance meter 80. NSMP, National Strong Motion Project; SW, southwest; NE, northeast; VE, vertical exaggeration.

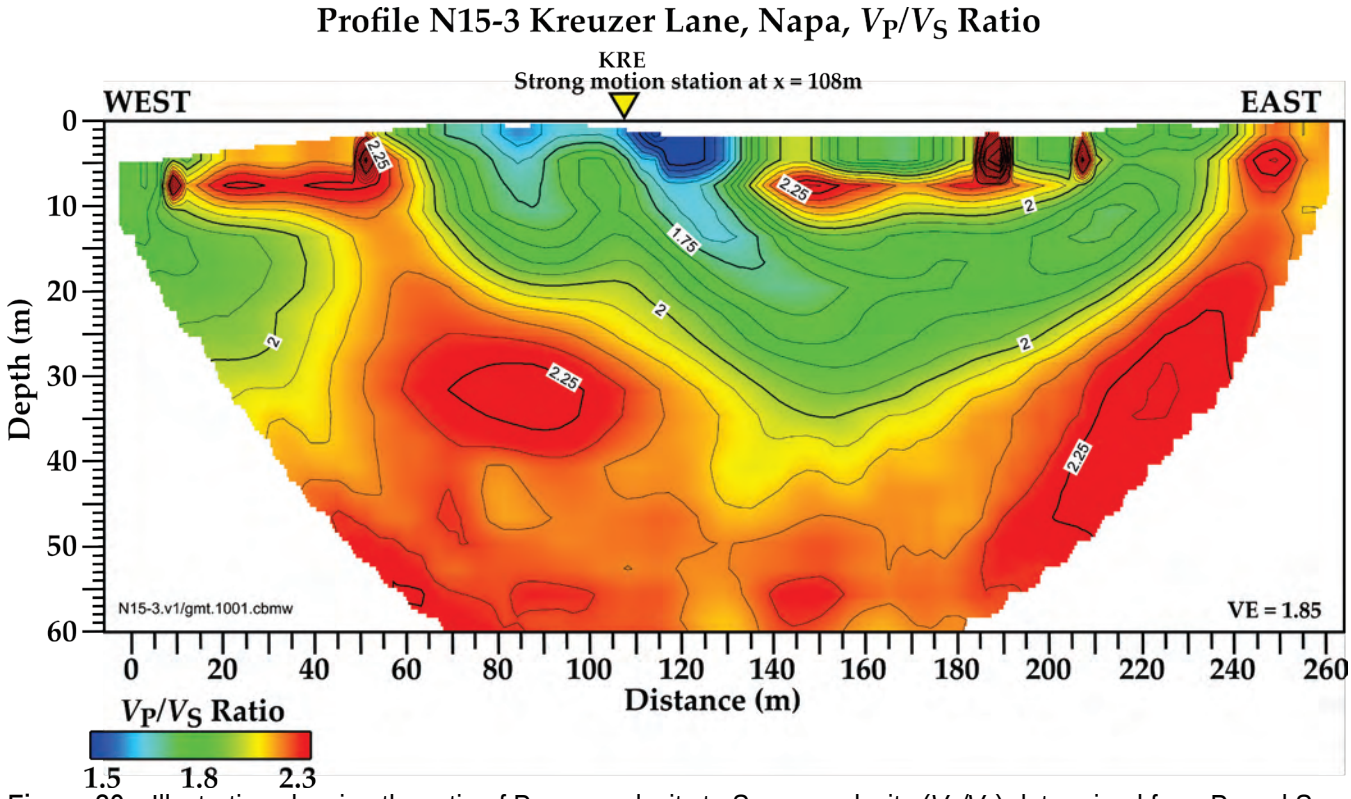

Figure 30. Illustration showing the ratio of P-wave velocity to S-wave velocity (V_P/V_S) determined from P- and S-wave refraction tomography along Kreuzer Lane (KRE), Napa County, California, seismic profile range from 1.5 to 2.3. The highest V_P/V_S ratios occur at discrete locations near the surface and at depth. VE, vertical exaggeration; m, meters.

Appendix 5—Poisson's Ratio Determined From P- and S-Wave Refraction Tomography

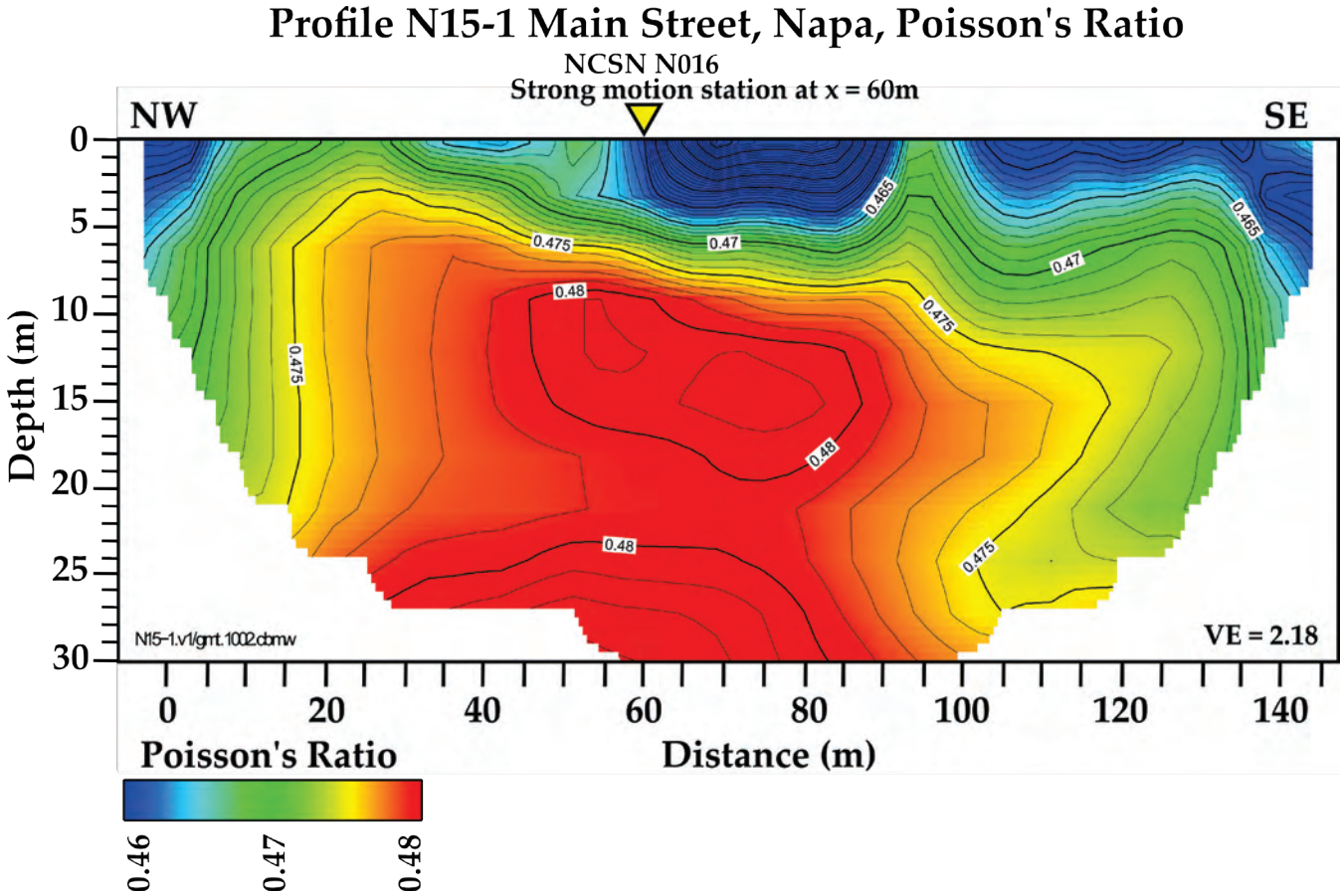

Figure 31. Illustration showing Poisson's ratio determined from P- and S-wave refraction tomography along Main Street in downtown Napa, California, seismic profile range from 0.43 to 0.48, which are indicative of a high level of water saturation along the entire seismic profile. NCSN, Northern California Seismic Network; NW, northwest; SE, southeast; VE, vertical exaggeration; m, meters.

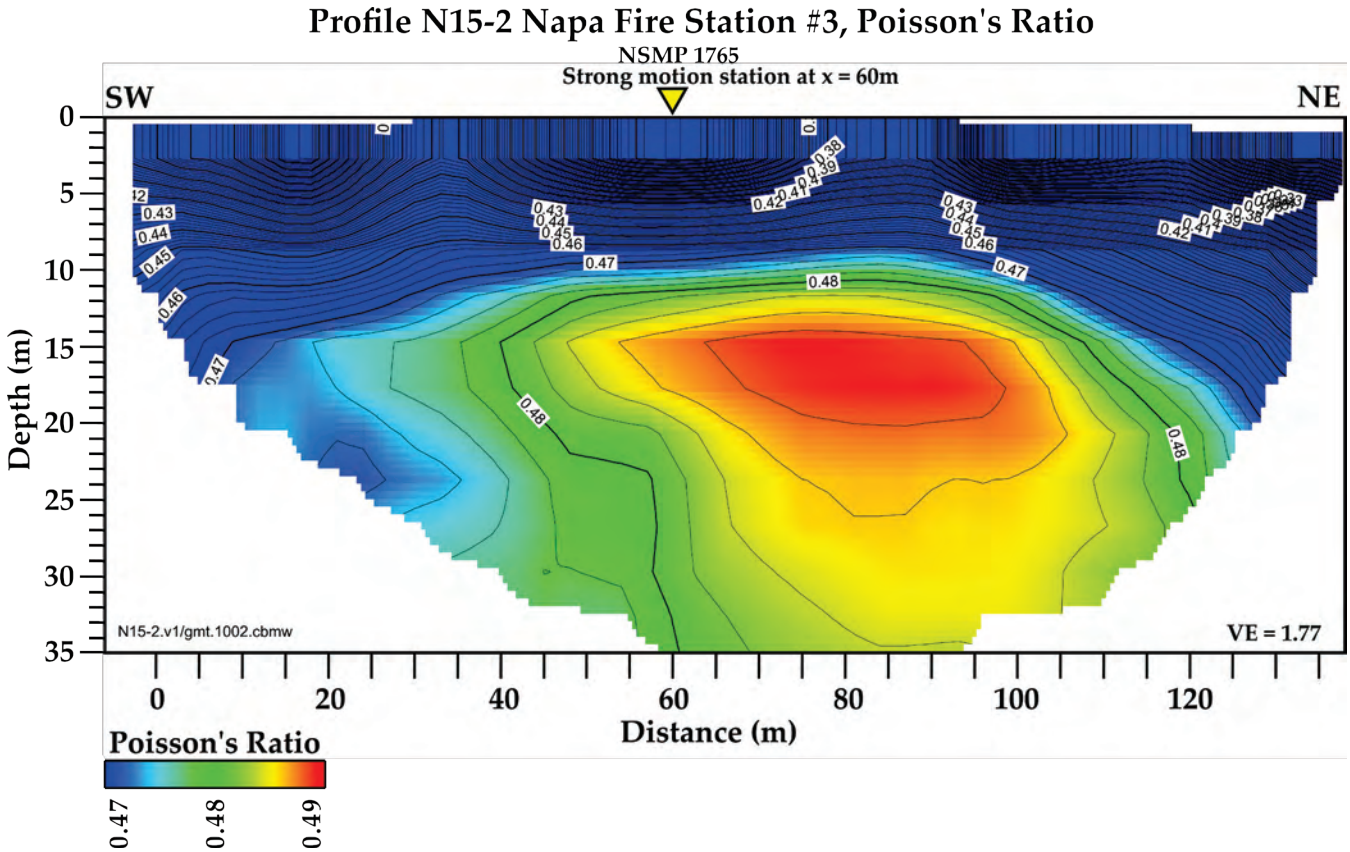

Figure 32. Illustration showing Poisson's ratio determined from P- and S-wave refraction tomography along Napa Fire Station 3, Napa County, California, seismic profile range from 0.30 to 0.49. The highest Poisson's ratio occurs below 12 meters (m) depth near the leaking water tower at distance meter 80. NSMP, National Strong Motion Project; SW, southwest; NE, northeast; VE, vertical exaggeration.

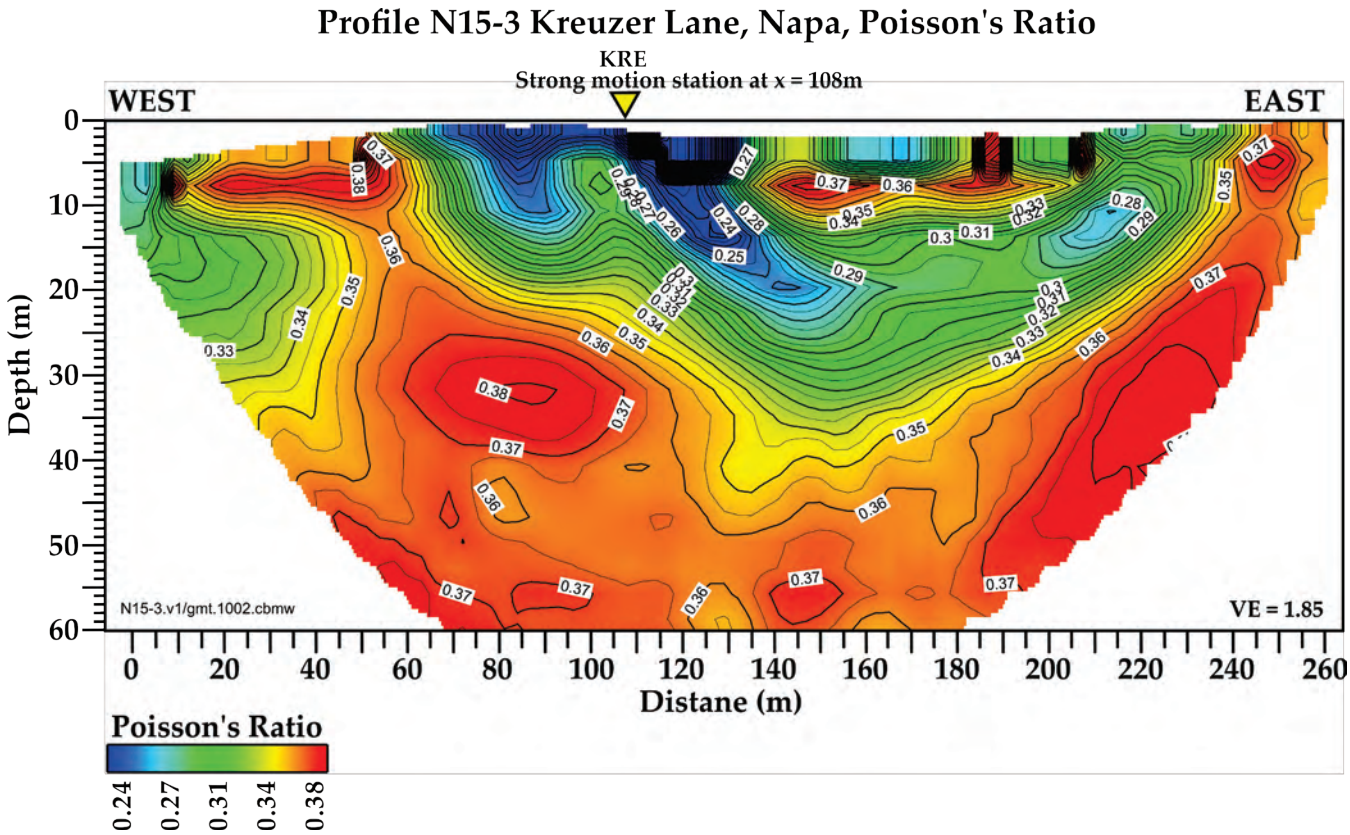

Figure 33. Illustration showing showing Poisson's ratio determined from P- and S-wave refraction tomography along Kreuzer Lane (KRE), Napa, California, seismic profile range from 0.24 to 0.38 and are highly variable along the lateral and vertical extent of the seismic profile. The relatively low Poisson's ratios suggest that there is not a laterally extensive zone of groundwater saturation along the seismic profile in the upper 60 meters (m) at the time of our seismic survey. VE, vertical exaggeration.

ISSN 2331-1258 (online)
https://doi.org/10.3133/ofr20181161